

# Quantum advantage from effective 200-qubit holographic random circuit sampling

Bingzhi Zhang<sup>1,†</sup> and Quntao Zhuang<sup>1,2,‡</sup>

<sup>1</sup>*Ming Hsieh Department of Electrical and Computer Engineering,*

*University of Southern California,*

*Los Angeles, California 90089, USA*

<sup>2</sup>*Department of Physics and Astronomy,*

*University of Southern California,*

*Los Angeles, California 90089, USA*

<sup>†</sup>*bingzhiz@usc.edu; <sup>‡</sup>qzhuang@usc.edu*

Quantum computers hold the promise of outperforming classical computers in solving certain problems. While large-scale quantum algorithms will require fault-tolerant devices, near-term demonstrations of quantum advantage on existing devices can provide important milestones. Random circuit sampling has emerged as a leading candidate for such demonstrations. However, existing implementations often underutilize circuit depth, limiting the achievable advantage. We introduce a holographic random circuit sampling algorithm that substantially increases the sampling complexity by leveraging repeated interactions and mid-circuit measurements. This approach scales the effective sampling dimension with the circuit depth, ultimately leading to an exponential growth in sampling complexity. With merely 20 physical qubits on IBM quantum devices, we experimentally demonstrate the effective sampling of up to 200 qubits, with a cross-entropy benchmark fidelity of 0.0593, establishing a new route to scalable quantum advantage through the combined use of spatial and temporal quantum resources.

## I. INTRODUCTION

Achieving quantum advantage is a central milestone in quantum science. Before fault-tolerant quantum computers can factor a large number [1, 2] or simulate a large quantum system [3, 4], near-term progress relies on alternative tasks tailored to current hardwares. Random circuit sampling (RCS) [5] has emerged as a leading method for demonstrating quantum supremacy and benchmarking quantum devices [6], with successful realizations across multiple platforms up to 83 qubits [7–12].

Despite these advances, existing RCS implementations underutilize a critical resource: circuit depth. Once the depth exceeds logarithmic scaling [13, 14], additional layers only marginally increase sampling complexity characterized by anticoncentration, limiting the achievable advantage. This raises a key question: can deep quantum circuits be harnessed to further enhance sampling complexity beyond conventional RCS?

We address this question by introducing holographic random circuit sampling (HRCS)—a sampling algorithm that integrates spatial resource (qubit count) and temporal resource (circuit depth) to exponentially amplify sampling complexity beyond conventional RCS. In HRCS, mid-circuit measurements convert temporal evolution into additional effective degrees of freedom, allowing circuit depth to holographically expand the sampling dimension. With merely 10 physical qubits used on IBM quantum devices, we experimentally demonstrate effective RCS of up to 85 qubits, with a cross-entropy benchmarking (XEB) [15–17] fidelity a factor of 3 higher than the current record reported in Ref. [11]. At 55 effective qubits, our XEB fidelity is an order of magnitude higher than Google’s 53-qubit landmark experiment [7]. Scaling to 20 physical qubits, HRCS achieves effective sampling

of 200 qubits with an XEB fidelity of 0.0593, establishing a new route to scalable quantum advantage through the combined use of spatial and temporal quantum resources.

## II. RANDOM CIRCUIT SAMPLING PROBLEM

As shown in Fig. 1a, in RCS, the quantum system of  $N$  qubits is initialized in a trivial product state, i.e.  $|0\rangle = |0\rangle^{\otimes N}$ , and a random unitary circuit  $U$  is applied on the system. Finally, one performs measurements in a fixed set of basis, i.e. the computational basis, on the output state and collects the corresponding measurement result  $x \in \{0, 1\}^N$ . In this regard, each measurement outcome appears with probability  $p(x) = |\langle x|U|0\rangle|^2$ .

A key ingredient and necessary condition for the hardness of RCS is the anticoncentration (AC) of the measurement distribution. For shallow circuits like constant-depth ones, due to the information lightcone, the output state is only supported on a few computational bases. As a result, the simulation of sampling from  $p(x)$  remains relatively easy. However, when the circuit depth increases and the unitary becomes complex,  $p(x)$  develops AC—widely supported over a number of bases exponential in the number of qubits, leading to a hard task for reproduction on classical devices. Indeed, it has been proven that the computation of  $p(x)$  for a typical Haar random unitary is an NP-hard problem [16].

To quantify AC, we consider the widely-adopted [13, 14, 18, 19] metric of collision probability (CP) defined by

$$Z = \sum_x p(x)^2. \quad (1)$$

Given a shallow quantum circuit, large values of CP

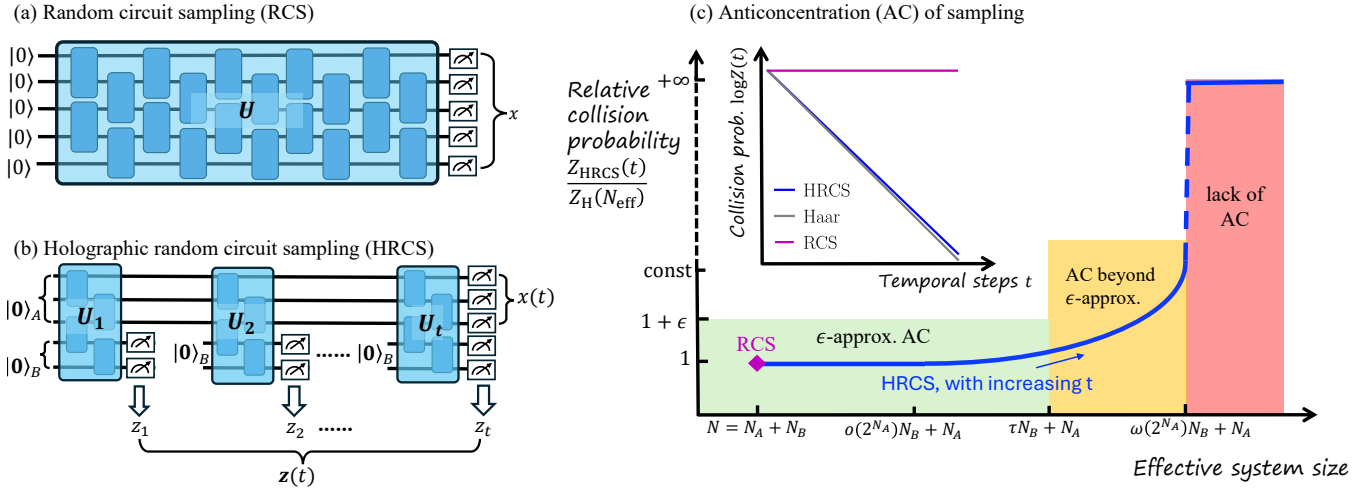


Figure 1. A schematic for quantum circuit sampling methods and main results. In (a) random circuit sampling (RCS), a random unitary circuit is applied on a trivial initial state and one performs computational basis measurements on the output state. (b) In holographic random circuit sampling (HRCS), computational basis measurements are performed on the bath  $B$  in each step following a unitary circuit, and on the system  $A$  in the end. The sampling task is targeted at the joint distribution of temporal mid-circuit measurements  $\mathbf{z}(t)$  and the final state measurements  $x(t)$ . In (c), we summarize the anticoncentration (AC) of sampling in HRCS in the asymptotic limit of  $N_A \rightarrow \infty$  for increasing effective system size in HRCS. While RCS is a single operating point (magenta diamond), HRCS allows the increase of effective system size (blue curve). The inset shows the decay of collision probability (in logarithmic scale) with increasing number of temporal steps.

indicate concentration—the corresponding RCS is easy. With the increase of layers of gates, the CP of an  $N$ -qubit state approaches the Haar value of

$$Z_H(N) = 2/(d+1) = 2/(2^N + 1), \quad (2)$$

inversely proportional to the system dimension  $d = 2^N$ , leading to a hard RCS problem [20].

The convergence of CP to the Haar value in Eq. (2) implies that, in a conventional RCS, the maximum attainable AC is solely determined by the system dimension, independent of circuit depth. In particular, recent results show that such a convergence happens at only a logarithmic-depth quantum circuit [13, 14]—going beyond logarithmic-depth does not seem to further enhance the complexity of RCS. This naturally poses a question: can a relatively small quantum system make use of a large quantum circuit depth to benefit RCS?

### III. HOLOGRAPHIC RANDOM CIRCUIT SAMPLING

In this work, we propose holographic random circuit sampling (HRCS) to go beyond the limitation of conventional RCS and benefit from deep quantum circuits.

As shown in Fig. 1b, HRCS adopts layers of quantum circuits  $U_1, U_2, \dots, U_t$  jointly on a system of  $N_A$  qubits and a bath of  $N_B$  qubits, interleaved with mid-circuit measurements on the bath to obtain measurement results, in addition to the final measurements on all qubits.

After each measurement, one can optionally choose reset or not reset the bath, as the unitaries are assumed to be random. Besides collecting the ‘temporal’ measurement results  $\mathbf{z}(t) = (z_1, \dots, z_t)$  throughout the measurements on bath, the final measurement on the system  $A$  gives additional ‘spatial’ contribution to the measurement results  $x(t)$ . The entire measurement outcome,  $\mathbf{z}(t)$  and  $x(t)$ , has an effective dimension of  $2^{N_{\text{eff}}(t)}$ , corresponding to  $N_{\text{eff}}(t) \equiv N_A + tN_B$  effective qubits growing with the number of rounds of mid-circuit measurements  $t$ .

Our main result is that AC remains for the  $2^{N_{\text{eff}}(t)}$ -dimensional measurement results up to an exponential time scale of  $t \sim 2^{N_A}$ , as sketched in Fig. 1c. As shown in the inset, the CP of the joint spatiotemporal sampling distribution  $P[\mathbf{z}(t), x(t)]$  in HRCS (blue solid) is close to the Haar value  $Z_H(N_A + tN_B)$  (gray solid); On the other hand, conventional RCS can only achieve  $Z_H(N_A + N_B)$  for a fixed constant number of qubits  $N_A + N_B$ , illustrated as the magenta curve. Therefore, HRCS is able to effectively utilize the ‘quantum volume’ of a device to exponentially increase the complexity of a sampling task.

Formally, we have the following theorem.

**Theorem 1** *For holographic random circuit sampling with each unitary  $U_t$  in 2-design, the ensemble-averaged collision probability at step  $t \geq 1$  is*

$$Z_{\text{HRCS}}(t) = \frac{2(d_A + 1)^{t-1}}{(1 + d_A d_B)^t}, \quad (3)$$

where  $d_A = 2^{N_A}, d_B = 2^{N_B}$  are Hilbert space dimensions

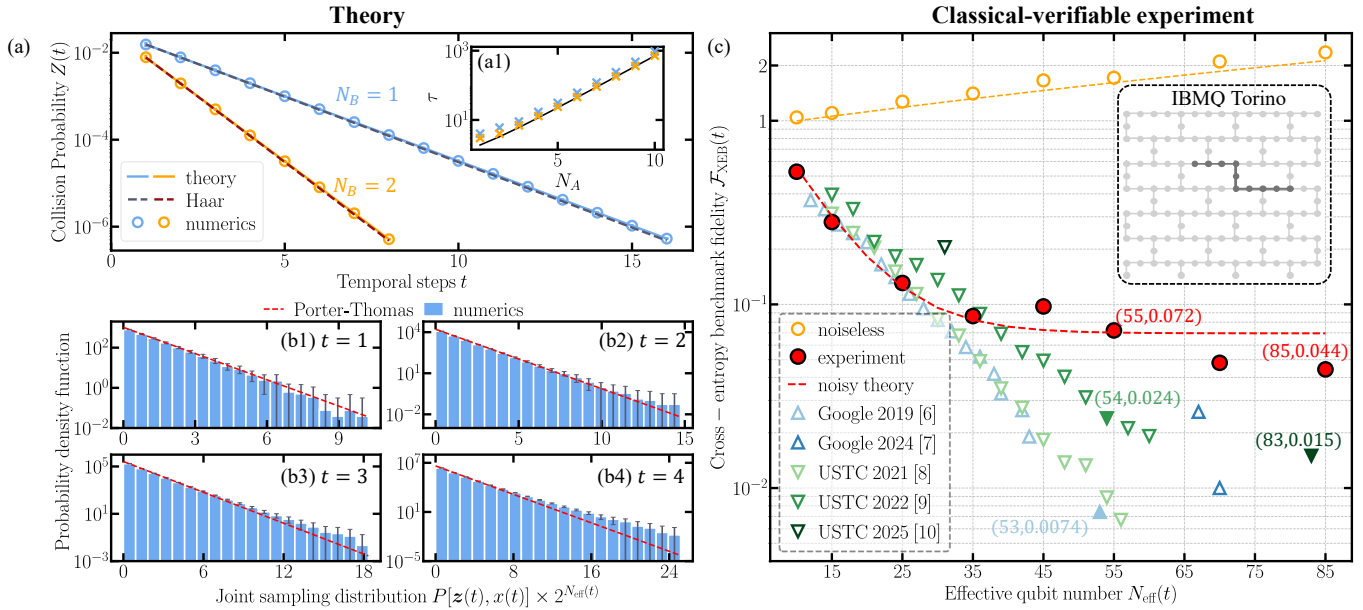


Figure 2. **Theory and Classical-verifiable benchmark of HRCS.** (a) Ensemble-averaged collision probability (CP)  $Z(t)$  for HRCS versus temporal steps in a system of  $N_A = 6$ ,  $N_B = 1, 2$  (blue and orange circles) qubits. Colored solid lines represent theoretical result of  $Z_{\text{HRCS}}(t)$  of Eq. (3) in Theorem 1. Dark-colored dashed lines are CP for Haar random states  $Z_H(N_{\text{eff}})$  in Eq. (2) with effective number of qubits  $N_{\text{eff}} = N_A + tN_B$ . Inset (a1) shows the growth of critical temporal steps  $\tau$  versus system size  $N_A$ , with  $\epsilon = 1$ . Blue and orange crosses represent numerical solutions of  $Z_{\text{HRCS}}(t) = (1 + \epsilon)Z_H(N_{\text{eff}})$  for  $N_B = 2$  and  $N_B = 6$  separately. The black line is Eq. (5). (b1-b4) Ensemble-averaged probability density function of the joint sampling distribution  $P[z(t), x(t)]$  in HRCS of  $N_A = 6$ ,  $N_B = 4$  qubits from  $t = 1$  to 4. Red dashed line is the Porter-Thomas distribution corresponding to Haar case. The ensemble average is over 50 HRCS instances with corresponding error bars. (d) Experimental verification of cross-entropy benchmark fidelity  $\mathcal{F}_{\text{XEB}}(t)$  in HRCS. Orange circles and dashed lines show the noiseless simulation of HRCS and theory. Red filled circles show HRCS experimental results on IBMQ Torino ( $t = 1, 2, 4, 6, 8, 10, 13, 16$ ) and red dashed line is the noisy theory prediction of Eq. (7). Each circuit in HRCS experiment is an 8-layer hardware-efficient ansatz of  $N_A = N_B = 5$  qubits. We perform  $10^6$  shots for sampling each circuit instance and each circle is an average over 10 instances. Dark grey circles in inset indicate the used qubits in experiments for  $t \leq 10$ . Blue up and green down triangles are known recent experiments from Google (2019 [7] and 2024 [8]) and USTC (2021 [9], 2022 [10] and 2025 [11]) for comparison. Data points for benchmarking are highlighted by color filling with  $(N_{\text{eff}}, \mathcal{F}_{\text{XEB}}(N_{\text{eff}}))$  specified.

of the system and bath. In the large-system limit  $d_A \gg 1$ ,

$$Z_{\text{HRCS}}(t) = Z_H(N_{\text{eff}}) \exp \left[ \frac{t(1 - d_B^{-1}) + d_B^{-t} - 1}{d_A} + \mathcal{O}\left(\frac{1}{d_A^2}\right) \right]. \quad (4)$$

At  $t = 1$ , both Eqs. (3) and (4) recover the RCS result in Eq. (2) for a system of  $N_A + N_B$  qubits. We emphasize that it is crucial to sample from the joint spatiotemporal distribution—marginal distributions are close to uniform (see Appendix D). In Fig. 2a, we verify Eq. (3) (solid) with numerical simulations (circles) where the CP exponentially decays with temporal steps  $t$ , for both  $N_B = 1$  (blue) and  $N_B = 2$  (orange). We also see that the CP of HRCS is close to the Haar results  $Z_H(N_{\text{eff}})$  in Eq. (2), depicted as the dashed lines. The effective number of qubits grows with the steps  $t$  and leads to small  $Z_{\text{HRCS}}(t)$ . The increasing effective sampling size  $N_{\text{eff}}(t) = N_A + tN_B$  indicates an increase of sampling complexity. However, such an increase does not last forever, as expected.

To understand the maximum complexity achievable by HRCS, we define the  $\epsilon$ -approximate Haar AC by  $Z_{\text{HRCS}}(t) \leq (1 + \epsilon)Z_H(N_{\text{eff}})$ , for an arbitrary constant  $\epsilon > 0$ . From Eq. (4),  $\epsilon$ -approximate Haar AC is satisfied when the number of temporal steps in HRCS (green region in Fig. 1c) is bounded by

$$t \leq \tau \equiv \frac{d_B}{d_B - 1} \left( \frac{1}{2} + d_A \log(1 + \epsilon) \right) \simeq \frac{1}{2} + d_A \log(1 + \epsilon). \quad (5)$$

Therefore,  $\epsilon$ -approximate AC survives at least until an exponentially large time scale  $t \sim o(2^{N_A})$ , leading to an effective system size  $o(2^{N_A})N_B + N_A$  exponential in  $N_A$ , as we illustrate in Fig. 1c. We verify the critical temporal steps  $\tau$  with numerical solutions of  $Z_{\text{HRCS}}(\tau) = (1 + \epsilon)Z_H(N_{\text{eff}})$  in Fig. 2a1, where we see the convergence toward a universal scaling of  $1/2 + 2^{N_A} \log(1 + \epsilon)$  as shown by the black line, with increasing  $N_B$  (blue to orange crosses).

Even at  $t > \tau$ , when  $t/2^{N_A} \leq c$  remains bounded by a constant, the sampled distribution in HRCS remains

AC, despite with a larger constant approximation error (yellow region in Fig. 1c). However, if  $t \sim \omega(2^{N_A})$  (red region), then  $Z_{\text{HRCS}}(t)/Z_{\text{H}}(N_{\text{eff}})$  grows with system size  $N_A$ , leading to the lack of AC.

We further confirm the above observation from CP via various statistical tools. We begin with a simple numerical check on the probability density of the joint distribution probability (PoP) in Fig. 2b1-b4 for sampling at different steps. The empirical PoP of  $P[\mathbf{z}(t), x(t)]$  (bars) for a system of  $N_A = 6, N_B = 4$  aligns closely with the Porter-Thomas distribution for Haar random outcomes of dimension  $2^{N_A+tN_B}$  (red dashed line) at all steps, up to small deviations in rare outcomes due to finite-size effect. As expected, the finite-size effect is more visible for larger  $t$  as the effective dimension increases. More formally, we can extend our analyses of CP in Theorem 1 to power sums for higher moments of the sampling distribution and the total variation distance to Haar sampling distribution, where similar conclusions are made (see Methods).

#### IV. EXPERIMENTAL VALIDATION

We experimentally implement HRCS on IBM quantum devices, with a first 10-qubit experiment in the classical-verifiable region and a second 20-qubit experiment going into the quantum supremacy region.

To verify the experimental results, we adopt the common tool of cross-entropy benchmarking (XEB) [15–17], which compares the frequency of measured bitstrings in experiments versus the corresponding ideal probability from classical simulation. For bitstrings with a total of  $N_{\text{eff}}(t) = N_A + tN_B$  bits being measured, the XEB fidelity can be obtained via

$$\mathcal{F}_{\text{XEB}} = 2^{N_{\text{eff}}(t)} \langle P(x_i) \rangle_i - 1, \quad (6)$$

where the average  $\langle \cdot \rangle_i$  is over the observed bitstrings  $x_i$  and  $P(x_i)$  is the probability of bitstring  $x_i$  computed from classical simulation of the ideal noiseless quantum circuit. When the experiment is entirely faithful to the ideal quantum circuit,  $\mathcal{F}_{\text{XEB}} = 2^{N_{\text{eff}}(t)} Z - 1$ , where  $Z$  is the CP defined in Eq. (1). For the exact Haar distribution,  $\mathcal{F}_{\text{XEB}} \simeq 1$ ; while a random uniform sampling independent of the quantum circuit leads to  $\mathcal{F}_{\text{XEB}} = 0$ .

For the ideal quantum circuit, Theorem 1 directly provides the prediction of XEB values. Due to the hardware noise, the experimental data are typically substantially lower than the ideal theory predictions. To characterize the noise effect on XEB fidelity, we develop a coarse-grained noise model by adding identical depolarizing channels  $\mathcal{N}(\rho) = \gamma\rho + (1-\gamma)\mathbf{I}/d$  onto the system and bath separately following each global unitary  $U_t$ . In the asymptotic limit of  $d_A, d_B \gg 1$ , we derive the noisy XEB fidelity as (see details and full formula in Appendix E)

$$\mathcal{F}_{\text{XEB}}(t) \simeq \gamma^{2t} \left( 1 + \frac{1-\gamma}{\gamma d_B} t \right) + \frac{\gamma}{(1-\gamma) d_A}. \quad (7)$$

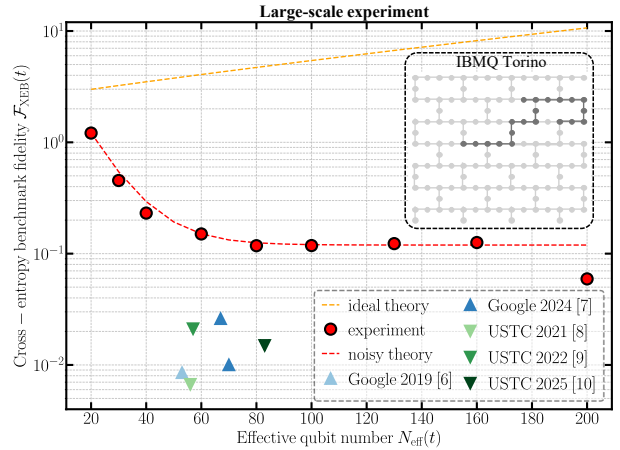


Figure 3. **Large-scale benchmark of HRCS.** Experimental verification of cross-entropy benchmark fidelity  $\mathcal{F}_{\text{XEB}}(t)$  in large-scale HRCS. Orange dashed line show the noiseless theory of HRCS. Red filled circles show experimental results of HRCS on IBMQ Torino ( $t = 1, 2, 3, 5, 7, 9, 12, 15, 19$ ) and red dashed line is the noisy theory prediction. The experiments utilizes 20 qubits in two patches. We perform  $10^6$  shots for sampling each circuit instance and each circle is an average over 10 circuit instances. Dark grey dots in inset show the used qubits on IBMQ Torino for one circuit instance at  $t = 19$ . Blue and green triangles represent the RCS results with largest size in known recent experiments from Google and USTC [7–11].

To showcase the capability of HRCS, we begin with only 10 qubits of IBMQ Torino:  $N_A = 5$  qubits for the system and  $N_B = 5$  qubits for the bath. The results are presented in Fig. 2c. As expected, the ideal XEB exhibits a slight growth with time step. Indeed, suppressed by system dimension, within the experimental accessible time steps up to  $t = 16$ , the growth is limited to a factor of 2, as indicated by the noiseless results in Fig. 2c (orange circle for simulation and orange dashed line for theory). Furthermore, our experimental data (red circles) demonstrate an initial exponential decay and late-time saturation, in good agreement with the asymptotic noisy theory of Eq. (7) (red dashed), with a single fitting parameter set  $\gamma = 0.69$ .

For a remarkable effective system of  $N_{\text{eff}}(t) \simeq 55$  qubits, our HRCS achieves XEB fidelity of 0.072 at  $t = 10$ , which is an order of magnitude higher than Google’s 2019 experiment [7] and a factor of at least three times higher than all previous experiments [7, 9, 10] (see details in Methods). Extending the effective system size, HRCS achieves XEB of 0.044 for  $N_{\text{eff}}(t) = 85$  qubits, at the time step of  $t = 16$ . This marks a factor of 3 higher XEB fidelity compared with the best comparable experiments on microwave superconducting devices: XEB of 0.015 for 83 qubits [11]. Considering that the XEB fidelity of ideal HCRS only increases by a factor of 1.7 and 2.3 for  $N_{\text{eff}} = 55, 85$ , the factors of 10 and 3 higher XEB of HRCS on IBMQ Torino indicate the advantage of HRCS, via exploiting both spatial and temporal re-

sources. Most importantly, instead of using 83 qubits, HRCS only adopts 10 physical qubits, marking a great spatial resource reduction.

We next implement HRCS with a larger number of 20 qubits to demonstrate quantum supremacy, with  $N_A = 10$  system qubits and  $N_B = 10$  bath qubits. To enable classical computation of the XEB fidelity in the experiment, we utilize the widely-adopted patch circuit method [7–12]—implementing two disjoint HRCS circuits simultaneously. Good agreement between the experimental data (red circles) and the noisy theory (red dashed line) persists, with a single fitting parameter of  $\gamma = 0.65$  slightly smaller than the 10-qubit experiment due to more qubits involved.

For  $N_{\text{eff}}(t) = 80$  effective qubits at  $t = 7$ , HRCS achieves a XEB fidelity of 0.118, which is nearly an order of magnitude higher than that in USTC’s 2025 experiment [11] of 83 qubits (dark green triangle in Fig. 3)—the largest scale RCS experiment on the superconducting platform so far. Meanwhile, the ideal HRCS XEB fidelity only increases by a factor of 4.7. We further extend the number of temporal steps in HRCS, and achieve XEB fidelity of 0.126 for  $N_{\text{eff}}(t) = 160$  and 0.0593 for  $N_{\text{eff}}(t) = 200$  qubits. Even in the  $t = 19$  case of HRCS experiment, the ideal XEB fidelity only increases moderately by a factor of 10.7, considering the  $N_{\text{eff}}(t) = 200$  effective qubits implemented with only 20 physical qubits by HRCS.

Comparing the XEB fidelity 0.0593 for  $N_{\text{eff}}(t) = 200$  in the 20-qubit experiment with 0.044 for  $N_{\text{eff}}(t) = 85$  in the 10-qubit experiment, we note that the mild increase of XEB for the larger experiment is remanent of the mild increase in the ideal XEB fidelity. This is evident from the fact that both experiments agree well with our noisy theory in Eq. (7), with similar depolarizing noise levels.

## V. DISCUSSION

HRCS utilizes depth to ‘holographically’ expand the sampled instance size, while maintaining a verifiable figure of merit (XEB). Such a notion of complexity is consistent with the metric of quantum volume as power of quantum circuits and also with the classical simulation cost of large quantum circuits. Consider a quantum circuit of  $n$  qubits and  $t$  depth, for an exact simulation based on state vectors, it takes  $O(2^n)$  memory and  $O(2^n t)$  time. However, such an approach fails quickly as the number of qubits increase. At the same time, keeping the precision high may take time much more than  $O(2^n t)$  as errors build up and suppression of error in the simulation becomes computationally infeasible, especially when the dynamics is chaotic. For large quantum systems beyond exact simulation, approximate approaches such as path-sum [21], matrix-product state [22] and tensor-network [23] have simulation cost exponential in time, due to the linear growth of entanglement generally form-

ing volume-law.

A few open questions are worth mentioning. We have assumed the unitaries in between mid-circuit measurements to be Haar random or at least unitary design, which generally require linear-depth. Similar reduction to logarithmic depth is plausible as in the case of conventional RCS [13, 14]. Meanwhile, according to the analysis from CP, we expect that the number of temporal steps  $t$  plays as an order parameter in the classical simulation complexity. When  $t \sim \omega(2^{N_A})$ , HRCS is an easy problem as its sampling distribution lacks AC, while for smaller  $t$ , HRCS might also be NP-hard though a rigorous proof on computational complexity and whether the transition point coincides remains open. As RCS can be utilized for quantum device benchmark, XEB of HRCS can potentially serve as a benchmark to include both the quality of mid-circuit measurements and unitary gates in the circuit. In the experimental perspective, HRCS could also benefit from all-to-all connections, high-fidelity operations and error detection in other quantum computing platforms [12, 24] to establish further enhanced performance.

## VI. METHODS

### A. Power sums and total variation distance

In the main text, we have mainly focused on the CP of the sampling distribution in HRCS; Here, we extend the analyses to other statistical metrics on the distributions, including power sums (PS) and total variation distance (TVD).

We begin with the  $K$ -th order PS, defined by

$$Z_{\text{HRCS}}^{(K)}(t) \equiv \sum_{\mathbf{z}(t), x(t)} P[\mathbf{z}(t), x(t)]^K, \quad (8)$$

where  $K \geq 1$  is an integer. Note that the  $K = 2$  case reduces to the CP definition in Eq. (1). Therefore, the following theorem is a direct generalization of Theorem 1 to higher-order statistical moments of the joint sampling distribution (see Appendix C for a proof).

**Theorem 2** *For holographic random circuit sampling with each unitary  $U_t$  in  $K$ -design, the ensemble-averaged  $K$ -th power sum at step  $t \geq 1$  is*

$$Z_{\text{HRCS}}^{(K)}(t) = K! d_A d_B^t \left( \frac{(d_A + K - 1)!}{(d_A - 1)!} \right)^{t-1} \left( \frac{(d_A d_B - 1)!}{(d_A d_B + K - 1)!} \right)^t, \quad (9)$$

where  $d_A = 2^{N_A}, d_B = 2^{N_B}$  are Hilbert space dimensions

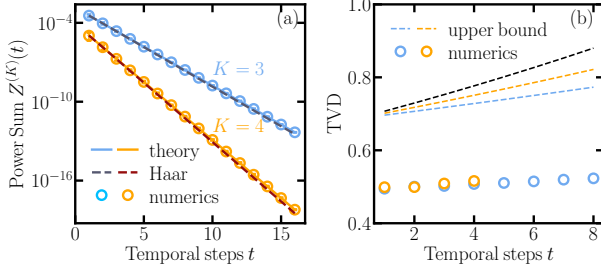


Figure 4. **Statistical measure for HRCS** (a) Ensemble-averaged power sums (PS)  $Z^{(K)}(t)$  for HRCS versus temporal steps in a system of  $N_A = 6, N_B = 1$  qubits with  $K = 3, 4$  (blue and orange circles). Colored solid lines represent theoretical results of Eq. (9) in Theorem 2. Dark-colored dashed lines are PS for Haar random states  $Z_H^{(K)}(N_{\text{eff}})$  with  $N_{\text{eff}} = N_A + tN_B$ . (b) Ensemble-averaged total variation distance (TVD) versus temporal steps  $t$  in a system of  $N_A = 4, N_B = 1, 2$  (blue and orange circles). Colored and black dashed lines represent the first and second upper bounds in Ineq. (12). In both subplots, we average over 50 HRCS circuit instances and in (b) we also average over 100 Haar random states.

of the system and bath. In the large-system limit  $d_A \gg 1$ ,

$$Z_{\text{HRCS}}^{(K)}(t) = Z_H^{(K)}(N_{\text{eff}}) \times \exp \left[ K(K-1) \frac{t(1-d_B^{-1}) + d_B^{-t} - 1}{2d_A} + \mathcal{O}\left(\frac{1}{d_A^2}\right) \right]. \quad (10)$$

Here the  $Z_H^{(K)}(N) = K! (2^N)! / (2^N + K - 1)!$  is the  $K$ -th power sum for  $N$ -qubit Haar random states.

It is expected that Eq. (9) with  $K = 2$  reduces to the exact CP result of Eq. (3) in Theorem 1, while for  $t = 1$ , Eq. (9) becomes the  $K$ -th PS of Haar random states  $Z_H^{(K)}(N)$  with system size  $N = N_A + N_B$  (see proof in Appendix B). Following the asymptotic form in Eq. (10), with the increase of temporal steps  $t$ , the  $K$ -th PS of HRCS  $Z_{\text{HRCS}}^{(K)}(t)$  deviates from the Haar one  $Z_H^{(K)}(N_{\text{eff}})$ ; however, the deviation is suppressed by the  $\sim K^2/d_A$  factor similar to Eq. (4). Therefore, the asymptotic scaling for CP in Fig. 1c also holds similarly for the  $K$ -th PS. In Fig. 4a, we verify our theory with numerical simulations (circles), and we also find the  $K$ -th PS of HRCS closely aligns with Haar results with the corresponding dimension (dashed). More precisely, for  $\epsilon$ -approximation Haar of  $K$ -th PS defined by  $Z_{\text{HRCS}}^{(K)}(t) \leq (1 + \epsilon)Z_H^{(K)}(N_{\text{eff}})$ , the largest temporal step  $\tau^{(K)} \simeq 1/2 + 2d_A \log(1 + \epsilon)/K(K-1)$  can be derived similarly to Eq. (5), as we detail in Appendix C. Due to the existence of  $K(K-1)$  in denominator, the  $\epsilon$ -approximation for  $K$ -th PS automatically implies the  $\epsilon$ -approximation for all  $K'$ -th PS with  $K' < K$ .

We next turn to the TVD to quantify the deviation of the statistics of HRCS sampling distribution from the

Haar statistics with the effective dimension. Unlike the noisy RCS study [18, 19] with the ensemble average over the random unitary circuit of RCS only, we instead consider the TVD averaged over both HRCS circuit instances  $C$  over the unitaries  $U_1, \dots, U_t$  and the Haar random unitary  $U$  in comparison as

$$\text{TVD} \equiv \frac{1}{2} \mathbb{E}_{\{U_k\} \in \text{Haar}} \mathbb{E}_{U \in \text{Haar}} \|P_C[\mathbf{z}(t), x(t)] - P_U[\mathbf{z}(t), x(t)]\|_1, \quad (11)$$

where  $P_C[\mathbf{z}(t), x(t)]$  is the joint distribution of HRCS circuit instance  $C$  and  $P_U[\mathbf{z}(t), x(t)]$  is the corresponding distribution of conventional Haar-random RCS with  $N_{\text{eff}}(t)$  qubits. We can prove the following inequality (see proof in Appendix C)

$$\text{TVD} \leq \frac{1}{2} \sqrt{2^{N_{\text{eff}}} Z_{\text{HRCS}}(t)} \leq \frac{1}{\sqrt{2}} \exp \left[ \frac{t-1}{2d_A} + \mathcal{O}\left(\frac{1}{d_A^2}\right) \right], \quad (12)$$

where the second inequality holds in the large-system limit similar to Eq. (4). This upper bound shows the statistical distance is suppressed exponentially by the dimension of the system and supports the time scale of  $\epsilon$ -approximate Haar AC in Ineq. (5). In Fig. 4b, we validate the above two theoretical bounds (colored dashed lines for the exact bound and black-dashed line for asymptotic bound) by comparing to the numerical simulations (circles) with various choices of bath size  $N_B$ . The small TVD also confirms the indistinguishability between output distributions of conventional RCS and HRCS, indicating the potential of HRCS for quantum cryptography and randomness certification [25].

## B. Details of experiments

We validate the XEB benchmark fidelity through experiments on the IBM quantum processor, Torino [26]. Below are additional details on the experiment.

In our experiment on real devices of  $B$  circuit instances with  $M$  shots for each instance, the XEB fidelity is estimated by

$$\hat{\mathcal{F}}_{\text{XEB}}(t) = \frac{2^{N_{\text{eff}}(t)}}{BM} \sum_{j=1}^B \sum_{i=1}^M P_{C_j}(x_i) - 1, \quad (13)$$

where  $P_{C_j}(x_i)$  is the ideal probability of obtaining bit string  $x_i$  from HRCS circuit instance  $C_j$ . Here we simulate the ideal HRCS circuit via `TensorCircuit` [27] on Nvidia A100 GPU.

In each step of HRCS experiment, to implement a random circuit mimicking a Haar random unitary, we adopt the one-dimensional hardware-efficient ansatz (HEA). An  $N$ -qubit,  $L$ -layer HEA circuit can be represented by

$$U_{\text{HEA}} = \prod_{\ell=1}^L W \otimes_{i=1}^N e^{-i\phi_{\ell,i}\hat{\sigma}_i^z/2} e^{-i\theta_{\ell,i}\hat{\sigma}_i^x/2}, \quad (14)$$

Error type	Average error rate
SX gate	$(3.07 \pm 1.27) \times 10^{-4}$
CZ gate	$(2.64 \pm 0.672) \times 10^{-4}$
Readout	$0.0214 \pm 0.0148$

Table I. Average error rates of the operations involved in our experiment on IBM Quantum Torino. As IBM Quantum implements RZ gate virtually in hardware via frame changes, it is error free. Calibration data are provided by IBM Quantum.

where  $W = \bigotimes_{i=1}^{\lfloor N/2 \rfloor} \text{CX}_{2i+1, 2i+2} \bigotimes_{i=1}^{\lfloor N/2 \rfloor} \text{CX}_{2i, 2i+1}$  is a fixed layer of CNOT gates on nearest neighbors in a brick-work style to build up entanglement among different qubits.  $\hat{\sigma}_i^x, \hat{\sigma}_i^z$  are the Pauli-X operator and Pauli-Z operator on  $i$ -th qubit, respectively, and the rotation angles  $\{\theta_{\ell, i}\}_{\ell, i}, \{\phi_{\ell, i}\}_{\ell, i}$  are uniformly distributed within  $[0, 4\pi]$ . Note that all of our gates are local to facilitate the experimental implementation. For the IBM Quantum Torino device we used, the naive gates are square root of X (SX), rotation-Z (RZ) and controlled-Z (CZ) gates. Therefore, circuit transpilation is implemented with highest level of optimization.

For the experiment in Fig. 2c, the  $L = 8$ -layer HEA circuit on  $N_A = 5, N_B = 5$  qubits involves 160 free parameters which is much less compared to the degree of freedom for the  $2^{10}$ -dimensional unitary, and 880 gates in total before transpilation. The number of gates in our transpiled circuits is presented in Appendix F. For the maximum of  $t = 16$  in this experiment, we use 5049 SX, 3684 RZ and 1152 CZ gates. Due to the automatic computing resource allocation from IBM Quantum service, for experiments with temporal steps  $t \leq 10$ , we utilize qubits in IBMQ Torino shown in dark grey circles in inset of Fig. 2c, and for  $t = 13, 16$ , we utilize slightly different qubits (see Fig. 9 in Appendix F). In Table I, we list the average error rates of all gates in our experiment and the readout errors for  $t \leq 10$ . The other case can be found in Appendix F.

In the quantum supremacy experiment of Fig. 3 with 20 physical qubits, exact simulation to obtain the ideal probability  $P_{C_j}(x_i)$  is beyond our computation power. Therefore, we consider the patch technique widely adopted in RCS experiments in the supremacy region [7].

Specifically, we adopt two patches of quantum circuits, each one can be classically simulated. In each patch, we use  $N'_A = 5$  qubits for the system and  $N'_B = 5$  qubits for the bath; In each step, the unitary is implemented via an 8-layer one-dimensional hardware-efficient ansatz, which is identical to the setup in classical-verifiable experiments of Fig. 2c. Therefore, we have twice the number of gates compared to Fig. 2c. For the maximum of  $t = 19$  in this experiment, we use 8748 SX, 11988 RZ and 2736 CZ gates with the number of gates for all circuits presented in Appendix F. Due to the allocation of qubit resources from Qiskit, the used qubits in each circuit instance of this experiments are slightly different from each other, however, we still expect a similar average error rate as shown in Table I. As we use the patch circuit method, both the ideal and noisy theory of XEB fidelity following from the single patch ones, as detailed in Appendix F. We list the key experimental results in Table II at  $t = 7, 15, 19$  for effective system of  $N_{\text{eff}} = 80, 160, 200$  qubits. At  $t = 7$ , our experiment of effective 80 qubits is about 8 times larger than USTC's result of 83 qubits [11]; More importantly, for HRCS experiments with further extended temporal steps, there does not exist comparable results in conventional RCS experiments.

In the end, we list the detailed circuit specifications of prior experiments used for benchmarking in Fig. 2c, to our best knowledge. We also list our XEB fidelity with a comparable effective system size in Table II for comparison. Although for small effective system sizes  $N_{\text{eff}} \simeq 15, 25$ , our XEB fidelity  $\mathcal{F}_{\text{XEB}}(t)$  of HRCS is relatively smaller than the one from conventional RCS due to more quantum gates involved in our small-scale circuits, with the increase of temporal steps thus effective system size  $N_{\text{eff}}$ , we see the XEB fidelity of HRCS outperforms the prior RCS experimental results by up to a factor of 10. With larger temporal steps, i.e. comparable to the system dimension  $2^{N_A}$ , we again see a suppression of the XEB performance improvements which might originate from the decoherence of system qubits. Therefore, it is important to identify the balance between the number of physical qubits  $N_A + N_B$  and the temporal steps  $t$  to maximize the performance of HRCS considering the current noisy intermediate-scale quantum computers at hand.

---

[1] P. W. Shor, in *Proceedings 35th annual symposium on foundations of computer science* (Ieee, 1994) pp. 124–134.

[2] P. W. Shor, SIAM review **41**, 303 (1999).

[3] R. P. Feynman, in *Feynman and computation* (cRc Press, 2018) pp. 133–153.

[4] S. Lloyd, Science **273**, 1073 (1996).

[5] D. Hangleiter and J. Eisert, Rev. Mod. Phys. **95**, 035001 (2023).

[6] N. Moll, P. Barkoutsos, L. S. Bishop, J. M. Chow, A. Cross, D. J. Egger, S. Filipp, A. Fuhrer, J. M. Gambetta, M. Ganzhorn, *et al.*, Quantum Science and Technology **3**, 030503 (2018).

[7] F. Arute, K. Arya, R. Babbush, D. Bacon, J. C. Bardin, R. Barends, R. Biswas, S. Boixo, F. G. Brandao, D. A. Buell, *et al.*, Nature **574**, 505 (2019).

[8] A. Morvan, B. Villalonga, X. Mi, S. Mandrà, A. Bengtsson, P. Klimov, Z. Chen, S. Hong, C. Erickson, I. Drozdov, *et al.*, Nature **634**, 328 (2024).

[9] Y. Wu, W.-S. Bao, S. Cao, F. Chen, M.-C. Chen,

Effective # of qubits $N_{\text{eff}}$	XEB fidelity $\mathcal{F}_{\text{XEB}}$		
	Prior work (Authors-# of qubits)	Our experiment (# of qubits)	Factor of improvement
10	0.3694 (Google2019-12Q)	0.5277 (10Q)	1.4285
15	0.3297 (Google2019-12Q)	0.2809 (10Q)	0.8520
	0.312 (USTC2021-15Q)		0.900
	0.396 (USTC2022-15Q)		0.709
25	0.1407 (Google2019-24Q)	0.1308 (10Q)	0.9296
	0.151 (USTC2021-24Q)		0.866
	0.183 (USTC2022-24Q)		0.715
35	0.05856 (Google2019-34Q)	0.08639 (10Q)	1.475
	0.05195 (Google2019-36Q)		1.663
	0.0491 (USTC2021-36Q)		1.76
	0.0888 (USTC2022-36Q)		0.973
45	0.01907 (Google2019-43Q)	0.09747 (10Q)	5.111
	0.0183 (USTC2021-45Q)		5.33
	0.0494 (USTC2022-45Q)		1.97
55	0.007406 (Google2019-53Q)	0.07215 (10Q)	9.742
	0.00889 (USTC2021-54Q)		8.12
	0.00671 (USTC2021-56Q)		10.8
	0.024 (USTC2022-54Q)		3.0
	0.0212 (USTC2022-57Q)		3.40
70	0.026 (Google2024-67Q)	0.04806 (10Q)	1.8
	0.01 (Google2024-70Q)		5
85	0.015 (USTC2025-83Q)	0.04427 (10Q)	3.0
80	0.015 (USTC2025-83Q)	0.1178 (20Q)	7.9
160	/		0.1258 (20Q)
200	/		0.0593 (20Q)

Table II. List of XEB fidelity from prior experiments of RCS [7–11] and our experiment from HRCS in Fig. 2c (top table) and Fig. 3 (bottom table). All prior RCS experiments to be benchmarked is performed on a two-dimensional superconducting quantum processor. In experiments Google2019 [7], USTC2021 [9] and USTC2022 [10] with corresponding 14, 10, 10 cycles, the XEB is evaluated with full circuit simulation, however in experiments Google2024 [8] and USTC2025 [11] with 16 cycles for each, the XEB is evaluated with 2 and 4-patch simplified circuits, respectively. The experimental data for Ref. [8–11] is estimated from corresponding figures in their manuscript, while the data of Ref. [7] is obtained from <https://doi.org/10.5061/dryad.k6t1rj8> directly.

X. Chen, T.-H. Chung, H. Deng, Y. Du, D. Fan, *et al.*, Phys. Rev. Lett. **127**, 180501 (2021).

[10] Q. Zhu, S. Cao, F. Chen, M.-C. Chen, X. Chen, T.-H. Chung, H. Deng, Y. Du, D. Fan, M. Gong, *et al.*, Science bulletin **67**, 240 (2022).

[11] D. Gao, D. Fan, C. Zha, J. Bei, G. Cai, J. Cai, S. Cao, F. Chen, J. Chen, K. Chen, *et al.*, Phys. Rev. Lett. **134**, 090601 (2025).

[12] M. DeCross, R. Haghshenas, M. Liu, E. Rinaldi, J. Gray, Y. Alexeev, C. H. Baldwin, J. P. Bartolotta, M. Bohn, E. Chertkov, J. Cline, J. Colina, D. DelVento, J. M. Dreiling, C. Foltz, J. P. Gaebler, T. M. Gatterman, C. N. Gilbreth, J. Giles, D. Gresh, A. Hall, A. Hankin, A. Hansen, N. Hewitt, I. Hoffman, C. Holliman, R. B. Hutson, T. Jacobs, J. Johansen, P. J. Lee, E. Lehman, D. Lucchetti, D. Lykov, I. S. Madjarov, B. Mathewson, K. Mayer, M. Mills, P. Niroula, J. M. Pino, C. Roman, M. Schechter, P. E. Siegfried, B. G. Tiemann, C. Volin, J. Walker, R. Shaydulin, M. Pistoia, S. A. Moses, D. Hayes, B. Neyenhuis, R. P. Stutz, and M. Foss-Feig, Phys. Rev. X **15**, 021052 (2025).

[13] B. Barak, C.-N. Chou, and X. Gao, arXiv:2005.02421 (2020).

[14] A. M. Dalzell, N. Hunter-Jones, and F. G. Brandão, PRX Quantum **3**, 010333 (2022).

[15] S. Boixo, S. V. Isakov, V. N. Smelyanskiy, R. Babbush, N. Ding, Z. Jiang, M. J. Bremner, J. M. Martinis, and H. Neven, Nature Physics **14**, 595 (2018).

[16] A. Bouland, B. Fefferman, C. Nirkhe, and U. Vazirani, Nature Physics **15**, 159 (2019).

[17] C. Neill, P. Roushan, K. Kechedzhi, S. Boixo, S. V. Isakov, V. Smelyanskiy, A. Megrant, B. Chiaro, A. Dunsworth, K. Arya, *et al.*, Science **360**, 195 (2018).

[18] A. M. Dalzell, N. Hunter-Jones, and F. G. Brandão, Communications in Mathematical Physics **405**, 78 (2024).

[19] B. Fefferman, S. Ghosh, M. Gullans, K. Kuroiwa, and

K. Sharma, PRX Quantum **5**, 030317 (2024).

[20] Note that  $Z = Z_H$  is the sweet spot for RCS complexity, as further smaller CP such as the extremely case of  $Z_{\text{uni}} = 1/d$  for a uniform distribution, RCS becomes simple again.

[21] S. Boixo, S. V. Isakov, V. N. Smelyanskiy, and H. Neven, arXiv:1712.05384 (2017).

[22] U. Schollwock, Emergent Phenomena in Correlated Matter (2013).

[23] I. L. Markov and Y. Shi, SIAM Journal on Computing **38**, 963 (2008).

[24] D. Bluvstein, S. J. Evered, A. A. Geim, S. H. Li, H. Zhou, T. Manovitz, S. Ebadi, M. Cain, M. Kalinowski, D. Hangleiter, *et al.*, Nature **626**, 58 (2024).

[25] M. Liu, R. Shaydulin, P. Niroula, M. DeCross, S.-H. Hung, W. Y. Kon, E. Cervero-Martín, K. Chakraborty, O. Amer, S. Aaronson, *et al.*, Nature **640**, 343 (2025).

[26] Q. Contributors, Zenodo: Geneva, Switzerland (2023).

[27] S.-X. Zhang, J. Allcock, Z.-Q. Wan, S. Liu, J. Sun, H. Yu, X.-H. Yang, J. Qiu, Z. Ye, Y.-Q. Chen, *et al.*, Quantum **7**, 912 (2023).

[28] B. Zhang, P. Xu, X. Chen, and Q. Zhuang, Nature Communications **16**, 6341 (2025).

[29] B. Zhang, F. Hu, R. Mo, T. Chen, H. E. Türeci, and Q. Zhuang, arXiv preprint arXiv:2506.22755 (2025).

[30] J. S. Cotler, D. K. Mark, H.-Y. Huang, F. Hernández, J. Choi, A. L. Shaw, M. Endres, and S. Choi, PRX quantum **4**, 010311 (2023).

[31] W. W. Ho and S. Choi, Phys. Rev. Lett. **128**, 060601 (2022).

## Acknowledgments.

Q.Z. and B.Z. acknowledge support from NSF (CCF-2240641, OMA-2326746, 2350153), ONR N00014-23-1-2296, AFOSR MURI FA9550-24-1-0349 and DARPA (HR0011-24-9-0362, HR00112490453, D24AC00153-02). The experiment was conducted using IBM Quantum Systems provided through USC's IBM Quantum Innovation Center.

## Appendix A: Quantum circuit sampling and anticoncentration

In this section, we introduce the circuit setup of holographic random circuit sampling (HRCS) and review the anticoncentration in quantum circuit sampling.

### 1. Setup of holographic random circuit sampling

We begin with the conventional random circuit sampling (RCS) that has been adopted to demonstrate quantum advantage [7, 9] (see Fig. 1a in the main text). Given a unitary quantum circuit  $U \in \mathcal{U}(2^N)$ , and a trivial  $N$ -qubit initial state  $|\mathbf{0}\rangle = |0\rangle^{\otimes N}$ , we can generally write out its output state from the circuit as

$$|\psi\rangle = U|\mathbf{0}\rangle. \quad (\text{A1})$$

One then performs a measurement on the output state  $|\psi\rangle$  in a fixed set of basis (i.e. computational basis), leading to the probability distribution

$$p_U(x) = |\langle x|U|\mathbf{0}\rangle|^2. \quad (\text{A2})$$

We review the analyses of conventional RCS in Appendix B.

In HRCS, a quantum system of  $N_A$  qubits (in initial state  $|\mathbf{0}\rangle_A$ ) repetitively interacts with a bath with  $N_B$  qubits (in initial state  $|\mathbf{0}\rangle_B$ ) via unitary circuits  $U_1, U_2, \dots, U_t$ . After the action of each unitary  $U_k$ , one performs a computational basis measurement on the bath, leading to the outcome  $z_k$ . For simplicity of description and theoretical analysis, we take the reset of the bath qubits back to  $|\mathbf{0}\rangle_B$  states before the next round of unitary interaction  $U_{k+1}$ , although our main results hold regardless reset or not (see proof in Appendix C). After the final unitary  $U_t$ , one measures the  $N_A$  system qubits in the computational basis to obtain the result  $x(t)$ , besides the bath measurement outcome  $z_t$ . Collecting all temporal measurement results  $\mathbf{z}(t) = (z_1, \dots, z_t)$  and the final ‘spatial’ measurement results  $x(t)$ , the joint probability of the spatiotemporal sampling

$$p_{\mathbf{U}}[\mathbf{z}(t), x(t)] = |\langle z_1|_{B_1} \cdots \langle z_t|_{B_t} \langle x(t)|_A U_t \cdots U_1 |\mathbf{0}\rangle_A |\mathbf{0}\rangle_{B_1} \cdots |\mathbf{0}\rangle_{B_t}|^2, \quad (\text{A3})$$

where we denote the unitary sequence in HRCS as  $\mathbf{U} = (U_1, \dots, U_t)$  and the bath system after reset in the  $k$ -th time step as  $B_k$ . Comparing the statistics in Eq. (A2) and Eq. (A3), the conventional RCS can be regarded as the  $t = 1$  special case of HRCS. Indeed, the length of the measurement outcome in HRCS,  $\mathbf{z}(t)$  and  $x(t)$ , increases with the time steps  $t$  as  $N_{\text{eff}} \equiv tN_B + N_A$  due to the reuse of the bath system. Although the probability of HRCS in Eq. (A3) seems to be a generalization of the probability for conventional RCS in Eq. (A2), it is indeed a non-unitary circuit due to mid-circuit measurements, shown in Fig. 1b in the main text. We present our analyses of HRCS in Appendix C.

As a comparison, one can also consider sampling from the marginal distributions, as we detail in Appendix D. In the case of spatial sampling, one samples  $x(t)$  from the marginal distribution  $p_{\mathbf{U}}[x(t)]$ ; In the case of temporal sampling, one samples only the mid-circuit measurement outcome  $\mathbf{z}(t)$  following the marginal distribution  $p_{\mathbf{U}}[\mathbf{z}(t)]$ .

### 2. Anticoncentration

The random circuit sampling problem asks how hard it is to classically simulate a distribution  $p_C(\cdot)$  generated from a quantum device  $C$ . For a typical state, when the distribution  $p_C(x)$  is widely supported over all computational basis  $|x\rangle$ , but not yet uniform over all basis, the sampling is expected to be a hard task. On the other hand, if the state is only supported on a limited number of basis, classical simulation could become efficient. Therefore, to characterize the spreading of a given discrete distribution, we consider the *anticoncentration* (AC) property, which is quantified by the collision probability (CP)

$$Z_C = \sum_x p_C(x)^2. \quad (\text{A4})$$

As a standard metric in the context of statistics, CP has already been widely utilized in the study of RCS, such as Refs. [14, 18, 19]. When  $Z_C$  is exponentially small in system size, the distribution is closer to uniform and therefore anticoncentrated; on the other hand, when  $Z_C = 1$ , the distribution is entirely concentrated on a single outcome. Indeed, CP also posts both lower and upper bounds on the maximum probability in the distribution by  $Z_C \leq \max_x p_C(x) \leq \sqrt{Z_C}$ . Note that CP is equivalent to the variance given a fixed mean, and it can also be

connected to the Rényi-2 entropy  $H_2[p_C(\cdot)]$  of the distribution via  $Z_C = e^{-H_2[p_C(\cdot)]}$ . In this regard, we also introduce higher-order moments to characterize the distribution—the higher-order power sums (PS)

$$Z_C^{(K)} = \sum_x p_C(x)^K. \quad (\text{A5})$$

In principle, the full information about the discrete-variable distribution  $p_C(\cdot)$  on  $D$ -dimensional support can be obtained from the collection  $\{Z_C^{(K)}\}_{K=1}^D$  via the Newton's identities up to a permutation on its supports.

In an RCS experiment, there is no preference on the choice of each quantum gate in the circuit. Therefore, we focus on the average-case performance of AC in this work, which is characterized by the ensemble-averaged collision probability as

$$Z = \mathbb{E}_{C \in \mathcal{C}}[Z_C], \quad (\text{A6})$$

where  $\mathcal{C}$  represents the ensemble of quantum circuit with a fixed architecture. Similarly, we also consider the ensemble-averaged PS  $Z^{(K)} = \mathbb{E}_{C \in \mathcal{C}}[Z_C^{(K)}]$ . When the dimension is large, we expect a small variance in  $Z_C$  among different circuit realizations, and one can also bound the CP in a typical circuit by the Markov inequality  $\mathbb{P}(Z_C \geq \alpha Z) \leq 1/\alpha$ .

For any discrete distribution  $p(\cdot)$  supported on a  $D$ -dimensional space, the CP is lower bounded by the value of the uniform distribution,  $Z \geq Z_{\text{uni}} = 1/D$ , which can also be regarded as the most anti-concentrated case, despite easy to sample classically. The distribution is regarded as “anticoncentrated” when  $Z/Z_{\text{uni}} \leq c$  with  $c$  to be a constant independent of the dimension  $D$ . In contrast, if  $Z/Z_{\text{uni}} = f(D)$  is an unbounded function depending on the dimension, it becomes “non-anticoncentrated” or lack of anticoncentration. The above criteria is also adopted in the study of RCS [14, 18]. Furthermore, the constraint on the CP can also be converted into the pointwise constraint by the Paley-Zygmund inequality, where AC with respect to  $Z$  also implies the AC of probability for each measurement outcome  $\mathbb{P}[p(\mathbf{x}) \geq \alpha/D] \geq (1 - \alpha)^2/(DZ)$  with  $\alpha \in [0, 1]$ , indicating a sufficient strong condition [19].

## Appendix B: Preliminary

In this section, we introduce the notations in Haar random unitary integration used in derivations of this work and take Haar random states in conventional RCS as a warm-up exercise.

### 1. Identities for Haar integral

We first introduce some important identities utilized in the following derivations of CP and PS in both Haar random states and HRCS. Let us begin with the doubled Hilbert space representation of operators. For an arbitrary operator  $\hat{A}$ , we define the doubled Hilbert space representation by

$$\hat{A} = \sum_{i,j} |i\rangle\langle j| \langle i|\hat{A}|j\rangle \rightarrow \hat{A} \rangle\langle = \sum_{i,j} \langle i|\hat{A}|j\rangle |i\rangle |j\rangle. \quad (\text{B1})$$

Therefore, when operator  $\hat{A}$  undergoing twirling by unitary  $U$ , we can write it in the doubled Hilbert space representation as

$$U \hat{A} U^\dagger \rightarrow [U \otimes U^*] \hat{A} \rangle\langle, \quad (\text{B2})$$

where  $U^*$  denotes the complex conjugate of  $U$ . This approach has also be utilized in prior works [28, 29]. With this notion, we can write the Hilbert-Schmidt inner product of two operators  $\hat{A}$  and  $\hat{B}$  simply as

$$\text{tr}(\hat{A}^\dagger \hat{B}) = \langle\langle \hat{A} | \hat{B} \rangle\rangle. \quad (\text{B3})$$

With the doubled Hilbert space representation, we can now introduce the identity for Haar unitary twirling as

$$\mathbb{E}_{\text{Haar}} \left[ (U \otimes U^*)^{\otimes K} \right] = \sum_{\sigma, \pi \in S_K} \text{Wg}_d(\sigma^{-1}\pi) |\hat{\sigma}\rangle\langle \hat{\pi}|, \quad (\text{B4})$$

where  $\sigma, \pi$  are permutations and  $S_K$  is the permutation group of  $K$  entries. Here  $\text{Wg}_d(\sigma^{-1}\pi)$  is the Weingarten function, defined as  $\text{Wg}_d(\sigma^{-1}\pi) = \left(d^{|\sigma^{-1}\pi|}\right)^{-1}$ , where  $|\sigma^{-1}\pi|$  denotes the number of cycles of the permutation  $\sigma^{-1}\pi$ . Specifically, in the case of  $K = 2$ , we have  $S_2 = \{e, \tau\}$  consisting of identity  $e$  and swap  $\tau$ . The above twirling identity can be explicitly written out as

$$\mathbb{E}_{\text{Haar}} \left[ (U \otimes U^*)^{\otimes 2} \right] = \frac{1}{d^2 - 1} (|\hat{e}\rangle \langle \hat{e}| + |\hat{\tau}\rangle \langle \hat{\tau}|) - \frac{1}{d(d^2 - 1)} (|\hat{e}\rangle \langle \hat{\tau}| + |\hat{\tau}\rangle \langle \hat{e}|). \quad (\text{B5})$$

In the end, we introduce another identity to be utilized in the evaluation of PS.

$$\sum_{\sigma \in S_K} \text{Wg}_d(\sigma) = \frac{(d-1)!}{(K+d-1)!}. \quad (\text{B6})$$

We also append a proof of Eq. (B6) here.

**Proof.** We first utilize the Haar twirling identity in Eq. (B4) and sandwich it by  $\langle \langle \mathbf{0} |$  and  $|\mathbf{0} \rangle \rangle$  to obtain

$$\langle \langle \mathbf{0} | \mathbb{E}_{\text{Haar}} \left[ (U \otimes U^*)^{\otimes K} \right] |\mathbf{0} \rangle \rangle = \sum_{\sigma, \pi \in S_K} \text{Wg}_d(\sigma^{-1}\pi) \langle \langle \mathbf{0} | \hat{\sigma} \rangle \rangle \langle \hat{\pi} | \mathbf{0} \rangle \rangle \quad (\text{B7})$$

$$= \sum_{\sigma, \pi \in S_K} \text{Wg}_d(\sigma^{-1}\pi) \quad (\text{B8})$$

$$= K! \sum_{\sigma \in S_K} \text{Wg}_d(\sigma), \quad (\text{B9})$$

where in the last line we utilize the property that  $S_K$  is closed and thus rename the dummy variable. Recall that we can also write  $\mathbb{E}_{\text{Haar}} \left[ (U \otimes U^*)^{\otimes K} \right] |\mathbf{0} \rangle \rangle$  as the  $K$ -th moment of Haar random states ensemble,

$$\langle \langle \mathbf{0} | \mathbb{E}_{\text{Haar}} \left[ (U \otimes U^*)^{\otimes K} \right] |\mathbf{0} \rangle \rangle = \text{tr} \left( |\mathbf{0}\rangle \langle \mathbf{0}|^{\otimes K} \int_{\text{Haar}} dU (U |\mathbf{0}\rangle \langle \mathbf{0}| U^\dagger)^{\otimes K} \right) \quad (\text{B10})$$

$$= \frac{(d-1)!}{(K+d-1)!} \sum_{\pi \in S_K} \text{tr} \left( |\mathbf{0}\rangle \langle \mathbf{0}|^{\otimes K} \hat{\pi} \right) \quad (\text{B11})$$

$$= \frac{K!(d-1)!}{(K+d-1)!}, \quad (\text{B12})$$

where the second line follows the definition of  $K$ -th moment of the Haar ensemble (see Refs. [28, 30, 31]). Comparing Eqs. (B9) and (B12), we can easily find

$$\sum_{\sigma \in S_K} \text{Wg}_d(\sigma) = \frac{(d-1)!}{(K+d-1)!}. \quad (\text{B13})$$

■

## 2. Sampling from Haar random states

In this section, we review the CP of Haar random states, studied in Ref. [14, 15], and extend to the  $K$ -th PS.

**Lemma 3** *The ensemble-averaged collision probability for sampling in  $N$ -qubit Haar random states is*

$$Z_{\text{H}}(N) = \frac{2}{2^N + 1}. \quad (\text{B14})$$

**Proof.** Here we provide two different approaches to prove Lemma 3 utilizing the Haar twirling identity and probability of probability (PoP) separately.

The ensemble averaged probability of measurement outcome  $x$  in Haar random states can be evaluated as

$$\begin{aligned} \mathbb{E}_{U \in \text{Haar}}[p_U(x)^2] &= \mathbb{E}_{U \in \text{Haar}}[|\langle x|U|\mathbf{0}\rangle|^4] \\ &= \mathbb{E}_{U \in \text{Haar}} \left[ \text{tr} \left( U^{\otimes 2} |\mathbf{0}\rangle\langle\mathbf{0}|^{\otimes 2} U^{\dagger \otimes 2} |x\rangle\langle x|^{\otimes 2} \right) \right] \end{aligned} \quad (\text{B15})$$

$$= \frac{1}{d^2 - 1} (\langle\langle x|\hat{e}\rangle\rangle \langle\langle \hat{e}|\mathbf{0}\rangle\rangle + \langle\langle x|\hat{\tau}\rangle\rangle \langle\langle \hat{\tau}|\mathbf{0}\rangle\rangle) - \frac{1}{d(d^2 - 1)} (\langle\langle x|\hat{e}\rangle\rangle \langle\langle \hat{\tau}|\mathbf{0}\rangle\rangle + \langle\langle x|\hat{\tau}\rangle\rangle \langle\langle \hat{e}|\mathbf{0}\rangle\rangle) \quad (\text{B16})$$

$$= \frac{2}{d^2 - 1} - \frac{2}{d(d^2 - 1)} = \frac{2}{d(d + 1)}, \quad (\text{B17})$$

where we utilize the twirling identity of Eq. (B5) in the third line and  $d = 2^N$  is the Hilbert space dimension. Here  $|\mathbf{0}\rangle\rangle, \langle\langle x|$  are the doubled Hilbert space representation of  $|\mathbf{0}\rangle\langle\mathbf{0}|^{\otimes 2}$  and  $|x\rangle\langle x|^{\otimes 2}$ , and  $\langle\langle x|\hat{\sigma}\rangle\rangle = 1$  for arbitrary  $x$  and  $\sigma \in S_2$ . Then following the definition, the ensemble-averaged collision probability is

$$Z_{\text{H}}(N) = \sum_x \mathbb{E}_{U \in \text{Haar}}[p_U(x)^2] = \frac{2}{d + 1}, \quad (\text{B18})$$

as there are in total  $d = 2^N$  different measurement outcomes.

Another method for proof follows from the known fact that the PoP for Haar random states follows Porter-Thomas (PT) distribution [15]

$$P(p_{\text{H}}(x) = p) = (d - 1)(1 - p)^{d-2}, \quad (\text{B19})$$

then the CP is simply the second moment of the PT distribution up to a constant multiplier as

$$Z_{\text{H}}(N) = d \mathbb{E}_{U \in \text{Haar}}[p_U(x)^2] = d \int_0^1 dp P(p_{\text{H}}(x) = p) p^2 = \frac{2}{d + 1}. \quad (\text{B20})$$

■ As  $Z_{\text{H}}(N) = 2/2^N + \mathcal{O}(1/4^N)$  in the large limit of  $N \gg 1$ , the measurement distribution is clearly anticoncentrated. We also would like to point out that it indeed only requires unitary of 2-design to achieve it.

Next, we extend to the  $K$ -th PS of full sampling in Haar random states.

**Lemma 4** *The ensemble-averaged  $K$ -th power sum in the sampling of  $N$ -qubit Haar random states is*

$$Z_{\text{H}}^{(K)} = \frac{K!d!}{(d + K - 1)!}, \quad (\text{B21})$$

where  $d = 2^N$  is the Hilbert space dimension.

The proof is similar to the one for CP.

**Proof.** We can utilize the Haar twirling identity in Eq. (B4) to evaluate the  $K$ -th power of measurement probability

$$\begin{aligned} \mathbb{E}_{U \in \text{Haar}}[p_U(x)^K] &= \mathbb{E}_{U \in \text{Haar}}[|\langle x|U|\mathbf{0}\rangle|^{2K}] \\ &= \mathbb{E}_{U \in \text{Haar}} \left[ \text{tr} \left( U^{\otimes K} |\mathbf{0}\rangle\langle\mathbf{0}|^{\otimes K} U^{\dagger \otimes K} |x\rangle\langle x|^{\otimes K} \right) \right] \end{aligned} \quad (\text{B22})$$

$$= \sum_{\sigma, \pi \in S_K} \text{Wg}_d(\sigma^{-1}\pi) \langle\langle x|\hat{\sigma}\rangle\rangle \langle\langle \hat{\pi}|\mathbf{0}\rangle\rangle \quad (\text{B23})$$

$$= \sum_{\sigma, \pi \in S_K} \text{Wg}_d(\sigma^{-1}\pi) \quad (\text{B24})$$

$$= \frac{K!(d - 1)!}{(d + K - 1)!}, \quad (\text{B25})$$

where we utilize the identity of sum of Weingarten functions in Eq. (B6). The  $K$ -th PS then becomes

$$Z_{\text{H}}^{(K)}(N) = \sum_x \mathbb{E}_{U \in \text{Haar}}[p_U(x)^K] = d \frac{K!(d - 1)!}{(d + K - 1)!} = \frac{K!d!}{(d + K - 1)!}. \quad (\text{B26})$$

We can also prove it utilizing the PoP directly.

$$Z_{\text{H}}^{(K)}(N) = d \mathbb{E}_{U \in \text{Haar}}[p_U(x)^K] = d \int_0^1 dp P(p_{\text{H}}(x) = p) p^K = \frac{K!d!}{(d + K - 1)!}. \quad (\text{B27})$$

■

### 3. Subsystem sampling in Haar random states

Finally, we show the sampling on a subsystem of Haar random states.

**Lemma 5** For a Haar random quantum state  $|\psi\rangle_{AB}$  in a bipartite system  $\mathcal{H} = \mathcal{H}_A \otimes \mathcal{H}_B$  with  $N = N_A + N_B$  qubits, the marginal sampling distribution  $p_{\text{Haar}}(x_B) = |\langle B | x_B | \psi \rangle_{AB}|^2$  follows the Beta distribution

$$\mathbb{P}[p_{\text{H}}(x_B) = p] = \text{Beta}(d_A, (d_B - 1)d_A), \quad (\text{B28})$$

where  $d_A = 2^{N_A}$ ,  $d_B = 2^{N_B}$  are the dimension of corresponding subsystems.

Note that in the limit of full sampling  $N_A \rightarrow 0$  thus  $d_A \rightarrow 1$ , the above Beta distribution converges to the Porter-Thomas distribution of  $d = d_B$ .

**Proof.** A Haar random state  $|\psi\rangle_{AB}$  can be written as  $|\psi\rangle_{AB} \propto \sum_{i_A, i_B} X_{i_A, i_B} |i_A\rangle_A |i_B\rangle_B$ , where the unnormalized amplitude  $X_{i_A, i_B} \sim \mathcal{CN}(0, \mathbf{I})$  follows a standard complex normal distribution, and thus the  $d_A \times d_B$  random matrix  $X$  follows complex Ginibre ensemble. After tracing out the subsystem  $A$ , we have the reduced state as

$$\begin{aligned} \rho_A &= \sum_{k_A} {}_A \langle k_A | \psi \rangle \langle \psi | k_A \rangle_A \\ &\propto \sum_{i_B, j_B} \sum_{k_A} X_{k_A, i_B} X_{k_A, j_B}^* |i_B\rangle \langle j_B|_B = \frac{X^T X^*}{\text{tr}(X^T X^*)}, \end{aligned} \quad (\text{B29})$$

which is a fixed traced Wishardt random matrix ensemble. Its diagonal elements form a normalized vector  $\mathbf{s} = (s_1, \dots, s_{d_B})^T$  where  $s_i = \sum_{i_A} |X_{i_A, i}|^2 \sim \text{Gamma}(d_A, 1)$  follows Gamma distribution. Then the normalized vector  $\mathbf{s}/(\sum_i s_i)$  follows the Dirichlet distribution as

$$\left( \frac{s_1}{\sum_i s_i}, \dots, \frac{s_{d_B}}{\sum_i s_i} \right)^T \sim \text{Dir}(d_A, \dots, d_A). \quad (\text{B30})$$

Note that the normalized vector corresponds to the diagonal entries of the reduced state  $\rho_A$ , and thus the probability of each sampling outcome. Therefore, the distribution of marginal sampling distribution is

$$\mathbb{P}[p_{\text{H}}(x_B) = p] = \text{Beta}(d_A, (d_B - 1)d_A). \quad (\text{B31})$$

■

**Corollary 6** The ensemble-averaged collision probability of the marginal sampling distribution  $p_{\text{H}}(x_B)$  of Haar random states is

$$Z_{\text{H}, B}(N_A, N_B) = \mathbb{E}_{U \in \text{Haar}} \left[ \sum_{x_B} p_U(x_B)^2 \right] = \frac{d_A + 1}{d_A d_B + 1}. \quad (\text{B32})$$

**Proof.** We can prove the CP by Haar twirling identity in Eq. (B5) as

$$Z_{\text{H}, B}(N_A, N_B) = d_B \mathbb{E}_{U \in \text{Haar}} [p_U(x_A)^2] \quad (\text{B33})$$

$$= d_B \mathbb{E}_{U \in \text{Haar}} \left[ \text{tr} \left( U^{\otimes 2} |\mathbf{0}\rangle \langle \mathbf{0}|^{\otimes 2} U^{\dagger \otimes 2} \mathbf{I}_A^{\otimes 2} \otimes |x_B\rangle \langle x_B|_B^{\otimes 2} \right) \right] \quad (\text{B34})$$

$$= \frac{d_B}{d^2 - 1} (\langle\langle x_B | \hat{e} \rangle\rangle_B \langle\langle \hat{e} | \hat{e} \rangle\rangle_A \langle\langle \hat{e} | \mathbf{0} \rangle\rangle + \langle\langle x_B | \hat{\tau} \rangle\rangle_B \langle\langle \hat{\tau} | \hat{\tau} \rangle\rangle_A \langle\langle \hat{\tau} | \mathbf{0} \rangle\rangle) \quad (\text{B35})$$

$$- \frac{d_B}{d(d^2 - 1)} (\langle\langle x_B | \hat{e} \rangle\rangle_B \langle\langle \hat{e} | \hat{e} \rangle\rangle_A \langle\langle \hat{\tau} | \mathbf{0} \rangle\rangle + \langle\langle x_B | \hat{\tau} \rangle\rangle_B \langle\langle \hat{e} | \hat{\tau} \rangle\rangle_A \langle\langle \hat{e} | \mathbf{0} \rangle\rangle) \quad (\text{B35})$$

$$= \frac{d_B}{d^2 - 1} (d_A^2 + d_A) - \frac{d_B}{d(d^2 - 1)} (d_A^2 + d_A) = \frac{d_A + 1}{d_A d_B + 1}. \quad (\text{B36})$$

The CP can also be proved utilizing the PoP from Lemma 5 as

$$Z_{\text{H}, B}(N_A, N_B) = d_B \int_0^1 dp P(p_{\text{H}}(x_B) = p) p^2 = \frac{d_A + 1}{d_A d_B + 1}. \quad (\text{B37})$$

One can easily show that the CP in Eq. (B32) is strictly upper bounded by  $Z_H$  of dimension  $d_B$  as  $Z_{H,B}(N_A, N_B) < Z_H(N_B)$  given a nontrivial subsystem  $A$  with  $d_A > 1$ . In large system size limit of  $d_A \gg 1$ , the CP for marginal sampling  $Z_{H,B}(N_A, N_B) = Z_{\text{uni}}(N_B)(1 + 1/d_A)$  converges to the uniform case of dimension  $2^{N_B}$ , up to finite-size corrections. The convergence of the marginal sampling of a subsystem in Haar random states toward the uniform distribution also hints a necessary condition for the emergent state design in random states generated via projective measurements on another subsystem, known as *deep thermalization* [30, 31].

### Appendix C: Spatiotemporal sampling in HRCS

In this section, we provide the proof to the theorems in the main text. Additionally, we present some numerical simulation results to verify the theorems. Before we start the proof, we first restate the theorems of the main text here for reader's convenience. The proof relies on an equivalent expansion of bath system at different temporal steps into a joint enlarged bath and postpone all mid-circuit measurements to the end, illustrated in Fig. 5a. For simplicity, we begin with the case where qubit reset is performed following every mid-circuit measurement; in the end, we show that the results remain the same regardless of reset or not reset.

#### 1. Proof of Theorem 1

**Theorem 7** (Theorem 1 in main text) *For holographic random circuit sampling with each unitary  $U_t$  in 2-design, the ensemble-averaged collision probability at step  $t \geq 1$  is*

$$Z_{\text{HRCS}}(t) = \frac{2(d_A + 1)^{t-1}}{(1 + d_A d_B)^t}, \quad (\text{C1})$$

where  $d_A = 2^{N_A}$ ,  $d_B = 2^{N_B}$  are Hilbert space dimensions of the system and bath. In the large-system limit  $d_A \gg 1$ ,

$$Z_{\text{HRCS}}(t) = Z_H(N_{\text{eff}}) \exp \left[ \frac{t(1 - d_B^{-1}) + d_B^{-t} - 1}{d_A} + \mathcal{O}\left(\frac{1}{d_A^2}\right) \right]. \quad (\text{C2})$$

It is proved as follows.

**Proof.** From the schematic in Fig. 5a, we first write out the joint probability of sampling  $\mathbf{z}(t), x(t)$  in the output state as

$$P_U[\mathbf{z}(t), x(t)] = \text{tr}(U |\mathbf{0}\rangle\langle\mathbf{0}|_{AB} U^\dagger |x(t), \mathbf{z}(t)\rangle\langle x(t), \mathbf{z}(t)|_{AB}), \quad (\text{C3})$$

where  $\mathbf{B} = (B_1, \dots, B_t)$  is the equivalent expanded bath system and  $|\mathbf{0}\rangle_{AB} = |\mathbf{0}_A, \mathbf{0}_{B_1}, \dots, \mathbf{0}_{B_t}\rangle$  is the initial state of the whole state. Here we denote  $U = \prod_{i=1}^t U_i$  as the global unitary of the equivalent circuit. The ensemble average of the squared probability becomes

$$\mathbb{E}_{U \in \text{Haar}} [P_U[\mathbf{z}(t), x(t)]^2] = \mathbb{E}_{U \in \text{Haar}} \text{tr} \left( U^{\otimes 2} |\mathbf{0}\rangle\langle\mathbf{0}|_{AB}^{\otimes 2} U^{\dagger \otimes 2} |x(t), \mathbf{z}(t)\rangle\langle x(t), \mathbf{z}(t)|_{AB}^{\otimes 2} \right) \quad (\text{C4})$$

$$= \langle\langle x(t), \mathbf{z}(t) |_{AB} \mathbb{E}_{U \in \text{Haar}} [U^{\otimes 2} \otimes U^{*\otimes 2}] |\mathbf{0}\rangle\langle\mathbf{0}|_{AB}, \quad (\text{C5})$$

where we utilize the doubled Hilbert space representation in the second line and omit the  $(\cdot)^{\otimes 2}$  in the doubled bra and ket. Now we evaluate Eq. (C5) step by step from  $U_1$  to  $U_t$ .

For the first step involving  $U_1$ , we have

$$\begin{aligned} & \langle\langle z_1(t) |_{B_1} \mathbb{E}_{U_1 \in \text{Haar}} [U_1^{\otimes 2} \otimes U_1^{*\otimes 2}] |\mathbf{0}\rangle\langle\mathbf{0}|_{AB_1} \\ &= \frac{1}{d^2 - 1} (\langle\langle z_1(t) | \hat{e} \rangle\langle \hat{e} |_{B_1} \langle\langle \hat{e} | \mathbf{0}\rangle\langle \mathbf{0}|_{AB_1} | \hat{e} \rangle\langle \hat{e} |_A + \langle\langle z_1(t) | \hat{\tau} \rangle\langle \hat{\tau} |_{B_1} \langle\langle \hat{\tau} | \mathbf{0}\rangle\langle \mathbf{0}|_{AB_1} | \hat{\tau} \rangle\langle \hat{\tau} |_A) \\ &= \frac{1}{d(d^2 - 1)} (\langle\langle z_1(t) | \hat{e} \rangle\langle \hat{e} |_{B_1} \langle\langle \hat{\tau} | \mathbf{0}\rangle\langle \mathbf{0}|_{AB_1} | \hat{e} \rangle\langle \hat{e} |_A + \langle\langle z_1(t) | \hat{\tau} \rangle\langle \hat{\tau} |_{B_1} \langle\langle \hat{e} | \mathbf{0}\rangle\langle \mathbf{0}|_{AB_1} | \hat{\tau} \rangle\langle \hat{\tau} |_A) \end{aligned} \quad (\text{C6})$$

$$= \frac{1}{d^2 - 1} (|\hat{e}\rangle\langle \hat{e}|_A + |\hat{\tau}\rangle\langle \hat{\tau}|_A) - \frac{1}{d(d^2 - 1)} (|\hat{e}\rangle\langle \hat{e}|_A + |\hat{\tau}\rangle\langle \hat{\tau}|_A) \quad (\text{C7})$$

$$= \frac{1}{d(d+1)} (|\hat{e}\rangle\langle \hat{e}|_A + |\hat{\tau}\rangle\langle \hat{\tau}|_A). \quad (\text{C8})$$

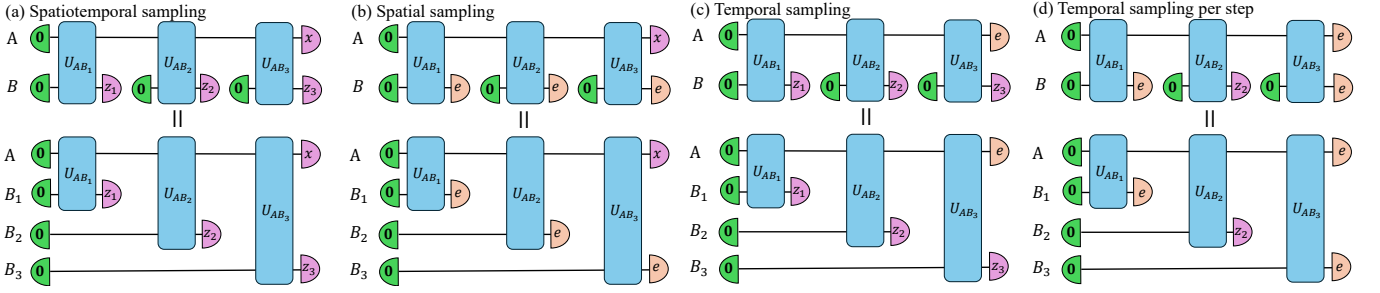


Figure 5. Schematic of the equivalent expansion of bath systems in HRCS for different sampling. Here we show an example of  $t = 3$ . In (d), we show the schematic for temporal sampling at the second step, with distribution  $p[z_2]$ .

As both permutations  $e, \tau$  from  $S_2$  appears, we next focus on the evolution of each of them separately under Haar random unitary.

$$\begin{aligned} & \langle\langle z_2(t) |_{B_2} \mathbb{E}_{U_2 \in \text{Haar}} [U_2^{\otimes 2} \otimes U_2^{*\otimes 2}] | \hat{e} \rangle\rangle_A |\mathbf{0}\rangle_{B_2} \\ &= \frac{1}{d^2 - 1} (\langle\langle z_2(t) | \hat{e} \rangle\rangle_{B_2} \langle\langle \hat{e} | \hat{e} \rangle\rangle_A \langle\langle \hat{e} | \mathbf{0} \rangle\rangle_{B_2} | \hat{e} \rangle\rangle_A + \langle\langle z_2(t) | \hat{\tau} \rangle\rangle_{B_2} \langle\langle \hat{\tau} | \hat{e} \rangle\rangle_A \langle\langle \hat{\tau} | \mathbf{0} \rangle\rangle_{B_2} | \hat{\tau} \rangle\rangle_A) \\ &\quad - \frac{1}{d(d^2 - 1)} (\langle\langle z_2(t) | \hat{e} \rangle\rangle_{B_2} \langle\langle \hat{\tau} | \hat{e} \rangle\rangle_A \langle\langle \hat{\tau} | \mathbf{0} \rangle\rangle_{B_2} | \hat{e} \rangle\rangle_A + \langle\langle z_2(t) | \hat{\tau} \rangle\rangle_{B_2} \langle\langle \hat{e} | \hat{e} \rangle\rangle_A \langle\langle \hat{e} | \mathbf{0} \rangle\rangle_{B_2} | \hat{\tau} \rangle\rangle_A) \end{aligned} \quad (\text{C9})$$

$$= \frac{1}{d^2 - 1} (d_A^2 |\hat{e}\rangle\rangle_A + d_A |\hat{\tau}\rangle\rangle_A) - \frac{1}{d(d^2 - 1)} (d_A |\hat{e}\rangle\rangle_A + d_A^2 |\hat{\tau}\rangle\rangle_A) \quad (\text{C10})$$

$$= \frac{d_A^2 d_B - 1}{d_B (d_A^2 d_B^2 - 1)} |\hat{e}\rangle\rangle_A + \frac{d_A (d_B - 1)}{d_B (d_A^2 d_B^2 - 1)} |\hat{\tau}\rangle\rangle_A. \quad (\text{C11})$$

Similarly, for  $\tau$ , we have

$$\begin{aligned} & \langle\langle z_2(t) |_{B_2} \mathbb{E}_{U_2 \in \text{Haar}} [U_2^{\otimes 2} \otimes U_2^{*\otimes 2}] | \hat{\tau} \rangle\rangle_A |\mathbf{0}\rangle_{B_2} \\ &= \frac{1}{d^2 - 1} (\langle\langle z_2(t) | \hat{e} \rangle\rangle_{B_2} \langle\langle \hat{e} | \hat{\tau} \rangle\rangle_A \langle\langle \hat{e} | \mathbf{0} \rangle\rangle_{B_2} | \hat{e} \rangle\rangle_A + \langle\langle z_2(t) | \hat{\tau} \rangle\rangle_{B_2} \langle\langle \hat{\tau} | \hat{\tau} \rangle\rangle_A \langle\langle \hat{\tau} | \mathbf{0} \rangle\rangle_{B_2} | \hat{\tau} \rangle\rangle_A) \\ &\quad - \frac{1}{d(d^2 - 1)} (\langle\langle z_2(t) | \hat{e} \rangle\rangle_{B_2} \langle\langle \hat{\tau} | \hat{\tau} \rangle\rangle_A \langle\langle \hat{\tau} | \mathbf{0} \rangle\rangle_{B_2} | \hat{e} \rangle\rangle_A + \langle\langle z_2(t) | \hat{\tau} \rangle\rangle_{B_2} \langle\langle \hat{e} | \hat{\tau} \rangle\rangle_A \langle\langle \hat{e} | \mathbf{0} \rangle\rangle_{B_2} | \hat{\tau} \rangle\rangle_A) \end{aligned} \quad (\text{C12})$$

$$= \frac{1}{d^2 - 1} (d_A |\hat{e}\rangle\rangle_A + d_A^2 |\hat{\tau}\rangle\rangle_A) - \frac{1}{d(d^2 - 1)} (d_A^2 |\hat{e}\rangle\rangle_A + d_A |\hat{\tau}\rangle\rangle_A) \quad (\text{C13})$$

$$= \frac{d_A (d_B - 1)}{d_B (d_A^2 d_B^2 - 1)} |\hat{e}\rangle\rangle_A + \frac{d_A^2 d_B - 1}{d_B (d_A^2 d_B^2 - 1)} |\hat{\tau}\rangle\rangle_A. \quad (\text{C14})$$

Until now, we have obtain all the mapping for the evolution of  $e, \tau$  under Haar ensemble of unitaries. For notation convenience, we use a 2-dimensional linear system to represent  $|\hat{e}\rangle\rangle_A, |\hat{\tau}\rangle\rangle_A$  and denote them as  $|\underline{0}\rangle \equiv |\hat{e}\rangle\rangle_A, |\underline{1}\rangle \equiv |\hat{\tau}\rangle\rangle_A$  though they do not form orthogonal bases. For initial condition of  $|\mathbf{0}\rangle_A$ , Eq. (C8) leads to  $|\mathbf{0}\rangle_A \rightarrow (|\underline{0}\rangle + |\underline{1}\rangle)/d(d+1)$ , which is taken to be the initial condition for evolution of this 2-dimensional linear system. The mapping in Eqs. (C11) and Eqs. (C14) can be represented by a  $2 \times 2$  matrix as

$$M = \frac{1}{d_B (d_A^2 d_B^2 - 1)} \begin{pmatrix} d_A^2 d_B - 1 & d_A (d_B - 1) \\ d_A (d_B - 1) & d_A^2 d_B - 1 \end{pmatrix}, \quad (\text{C15})$$

and the ensemble-averaged squared probability in Eq. (C5) becomes

$$\mathbb{E}_{U \in \text{Haar}} [P_U[\mathbf{z}(t), x(t)]^2] = \frac{1}{d(d+1)} [(\langle\langle \underline{0} | M^{t-1} (|\underline{0}\rangle + |\underline{1}\rangle) \rangle\langle x(t) | \hat{e} \rangle\rangle_A + (\langle\langle \underline{1} | M^{t-1} (|\underline{0}\rangle + |\underline{1}\rangle) \rangle\langle x(t) | \hat{\tau} \rangle\rangle_A)] \quad (\text{C16})$$

$$= \frac{2}{d(d+1)} \left( \frac{1 + d_A}{d_A d_B^2 + d_B} \right)^{t-1}. \quad (\text{C17})$$

Therefore, the ensemble-averaged CP is

$$Z_{\text{HRCS}}(t) = \sum_{x(t), \mathbf{z}(t)} \mathbb{E}_{U \in \text{Haar}} [P_U[\mathbf{z}(t), x(t)]^2] \quad (\text{C18})$$

$$= \frac{2d_A d_B^t}{d(d+1)} \left( \frac{1+d_A}{d_A d_B^2 + d_B} \right)^{t-1} \quad (\text{C19})$$

$$= \frac{2(1+d_A)^{t-1}}{(d_A d_B + 1)^t}, \quad (\text{C20})$$

which is Eq. (C1) in Theorem 7.

In the following, we derive the asymptotic expression of CP in HRCS in the large system limit of  $d_A \gg 1$ . Recall that the CP for Haar random states is  $Z_{\text{H}}(N_{\text{eff}}) = 2/(d_A d_B^t + 1)$  (see Eq. (B14) with  $N_{\text{eff}} = N_A + tN_B$ ). The CP ratio between Eq. (C1) of HRCS and Haar one becomes

$$\frac{Z_{\text{HRCS}}(t)}{Z_{\text{H}}(N_{\text{eff}})} = \frac{2(d_A + 1)^{t-1}}{(1 + d_A d_B)^t} \frac{d_A d_B^t + 1}{2} \quad (\text{C21})$$

$$= \frac{d_A^{t-1} d_A d_B^t}{(d_A d_B)^t} \left(1 + \frac{1}{d_A}\right)^{t-1} \left(1 + \frac{1}{d_A d_B^t}\right) \left(1 + \frac{1}{d_A d_B}\right)^{-t} \quad (\text{C22})$$

$$= \exp \left[ (t-1) \log \left(1 + \frac{1}{d_A}\right) + \log \left(1 + \frac{1}{d_A d_B^t}\right) - t \log \left(1 + \frac{1}{d_A d_B}\right) \right] \quad (\text{C23})$$

$$= \exp \left[ \frac{t(1 - d_B^{-1}) + d_B^{-t} - 1}{d_A} + \mathcal{O}\left(\frac{1}{d_A^2}\right) \right]. \quad (\text{C24})$$

Therefore, the asymptotic form of  $Z_{\text{HRCS}}(t)$  becomes

$$Z_{\text{HRCS}}(t) = Z_{\text{H}}(N_{\text{eff}}) \exp \left[ \frac{t(1 - d_B^{-1}) + d_B^{-t} - 1}{d_A} + \mathcal{O}\left(\frac{1}{d_A^2}\right) \right]. \quad (\text{C25})$$

■ For  $\epsilon$ -approximate Haar AC in terms of CP, we can directly solve  $Z_{\text{HRCS}}(t) \leq (1 + \epsilon)Z_{\text{H}}(N_{\text{eff}})$  to find the critical number of temporal steps. However, to obtain a intuitive and informative solution, we first upper bound the asymptotic form of Eq. (C2) by

$$\begin{aligned} Z_{\text{HRCS}}(t) &= Z_{\text{H}}(N_{\text{eff}}) \exp \left[ \frac{t(1 - d_B^{-1}) + d_B^{-t} - 1}{d_A} + \mathcal{O}\left(\frac{1}{d_A^2}\right) \right] \\ &\leq Z_{\text{H}}(N_{\text{eff}}) \exp \left[ \frac{t(1 - d_B^{-1}) - 1/2}{d_A} + \mathcal{O}\left(\frac{1}{d_A^2}\right) \right], \end{aligned} \quad (\text{C26})$$

where we utilize  $d_B^{-t} \leq d_B^{-1} \leq 1/2$ , and the corresponding critical temporal steps can be simply solved as

$$t \leq \tau \equiv \frac{d_B}{d_B - 1} \left( d_A \log(1 + \epsilon) + \frac{1}{2} \right), \quad (\text{C27})$$

which is Eq. (5) in the main text.

## 2. Proof of Theorem 2

**Theorem 8** (Theorem 2 in the main text) *For holographic random circuit sampling with each unitary  $U_t$  in  $K$ -design, the ensemble-averaged  $K$ -th power sum at step  $t \geq 1$  is*

$$Z_{\text{HRCS}}^{(K)}(t) = K! d_A d_B^t \left( \frac{(d_A + K - 1)!}{(d_A - 1)!} \right)^{t-1} \left( \frac{(d_A d_B - 1)!}{(d_A d_B + K - 1)!} \right)^t, \quad (\text{C28})$$

where  $d_A = 2^{N_A}$ ,  $d_B = 2^{N_B}$  are Hilbert space dimensions of the system and bath. In the large-system limit  $d_A \gg 1$ ,

$$Z_{\text{HRCS}}^{(K)}(t) = Z_{\text{H}}^{(K)}(N_{\text{eff}}) \exp \left[ K(K-1) \frac{t(1-d_B^{-1}) + d_B^{-t} - 1}{2d_A} + \mathcal{O}\left(\frac{1}{d_A^2}\right) \right]. \quad (\text{C29})$$

Here the  $Z_{\text{H}}^{(K)}(N) = K! (2^N)! / (2^N + K - 1)!$  is the  $K$ -th power sum for  $N$ -qubit Haar random states.

The proof is similar to Theorem 7.

**Proof.** The joint probability of sampling  $\mathbf{z}(t)$  and  $x(t)$  still follows Eq. (C3), and according to definition of  $K$ -th PS (Eq. (A5)), the ensemble-averaged  $K$ -th power of  $p[\mathbf{z}(t), x(t)]$  becomes

$$\mathbb{E}_{U \in \text{Haar}} [P_U[\mathbf{z}(t), x(t)]^K] = \mathbb{E}_{U \in \text{Haar}} \text{tr} \left( U^{\otimes K} |\mathbf{0}\rangle\langle\mathbf{0}|_{AB}^{(K)} U^{\dagger \otimes K} |x(t), \mathbf{z}(t)\rangle\langle x(t), \mathbf{z}(t)|_{AB}^{(K)} \right) \quad (\text{C30})$$

$$= \langle\langle x(t), \mathbf{z}(t) |_{AB} \mathbb{E}_{U \in \text{Haar}} [U^{\otimes K} \otimes U^{*\otimes K}] |\mathbf{0}\rangle\langle\mathbf{0}|_{AB}, \quad (\text{C31})$$

where we omit the  $(\cdot)^{\otimes K}$  in the doubled bra and ket. We then evaluate Eq. (C31) through all unitaries from  $U_1$  to  $U_t$ . For the first step involving  $U_1$ , we have

$$\begin{aligned} & \langle\langle z_1(t) |_{B_1} \mathbb{E}_{U_1 \in \text{Haar}} [U_1^{\otimes K} \otimes U_1^{*\otimes K}] |\mathbf{0}\rangle\langle\mathbf{0}|_{AB_1} \\ &= \langle\langle z_1(t) |_{B_1} \left[ \sum_{\sigma, \pi \in S_K} \text{Wg}_d(\sigma^{-1}\pi) |\sigma\rangle\langle\pi| \right] |\mathbf{0}\rangle\langle\mathbf{0}|_{AB_1} \end{aligned} \quad (\text{C32})$$

$$= \sum_{\sigma, \pi \in S_K} \text{Wg}_d(\sigma^{-1}\pi) |\sigma\rangle\langle\sigma|_A \quad (\text{C33})$$

$$= \sum_{\sigma \in S_K} |\sigma\rangle\langle\sigma|_A \left( \sum_{\pi \in S_K} \text{Wg}_d(\sigma^{-1}\pi) \right) = \frac{(d-1)!}{(K+d-1)!} \sum_{\sigma \in S_K} |\sigma\rangle\langle\sigma|_A, \quad (\text{C34})$$

where in the second line we utilize Haar unitary twirling of Eq. (B4), and in the last line, we utilize the identity in Eq. (B6). Now we can regard the sum of all permutations  $\sum_{\sigma \in S_K} |\sigma\rangle\langle\sigma|_A$  as a single entry and evaluate its evolution under the twirling of Haar random unitary  $U_2$

$$\begin{aligned} & \langle\langle z_2(t) |_{B_2} \mathbb{E}_{U_2 \in \text{Haar}} [U_2^{\otimes K} \otimes U_2^{*\otimes K}] \left( \sum_{\sigma \in S_K} |\sigma\rangle\langle\sigma|_A \right) |\mathbf{0}\rangle\langle\mathbf{0}|_{B_2} \\ &= \langle\langle z_2(t) |_{B_2} \left[ \sum_{\pi, \pi' \in S_K} \text{Wg}_d(\pi^{-1}\pi') |\pi\rangle\langle\pi'| \right] \left( \sum_{\sigma \in S_K} |\sigma\rangle\langle\sigma|_A \right) |\mathbf{0}\rangle\langle\mathbf{0}|_{B_2} \end{aligned} \quad (\text{C35})$$

$$= \sum_{\pi, \pi' \in S_K} \text{Wg}_d(\pi^{-1}\pi') |\pi\rangle\langle\pi|_A \langle\langle z_2(t) | \pi \rangle\langle\pi|_{B_2} \sum_{\sigma \in S_K} \langle\langle \pi' | \sigma \rangle\langle\pi' | \sigma \rangle\langle\sigma|_A \langle\langle \pi' | \mathbf{0} \rangle\langle\mathbf{0}|_{B_2} \quad (\text{C36})$$

$$= \sum_{\pi, \pi' \in S_K} \text{Wg}_d(\pi^{-1}\pi') |\pi\rangle\langle\pi|_A \left( \sum_{\sigma \in S_K} d_A^{|\pi'^{-1}\sigma|} \right) \quad (\text{C37})$$

$$= \sum_{\pi, \pi' \in S_K} \text{Wg}_d(\pi^{-1}\pi') |\pi\rangle\langle\pi|_A \frac{(d_A + K - 1)!}{(d_A - 1)!} \quad (\text{C38})$$

$$= \frac{(d_A + K - 1)!(d - 1)!}{(d_A - 1)!(d + K - 1)!} \sum_{\sigma \in S_K} |\sigma\rangle\langle\sigma|_A, \quad (\text{C39})$$

where the second to last line we utilize the definition of Stirling numbers of the first kind which leads to the falling factorial. From Eq. (C39), we find that the input entry  $\sum_{\sigma \in S_K} |\sigma\rangle\langle\sigma|_A$  is exactly reproduced, which is expected as the sum of all permutation elements remains invariant under twirling of Haar unitary. Therefore, we can evaluate Eq. (C31) utilizing Eq. (C34) and (C39) as

$$\mathbb{E}_{U \in \text{Haar}} [P_U[\mathbf{z}(t), x(t)]^K] = \left( \frac{(d_A + K - 1)!(d - 1)!}{(d_A - 1)!(d + K - 1)!} \right)^{t-1} \frac{(d - 1)!}{(d + K - 1)!} \langle\langle x(t) | \sum_{\sigma \in S_K} |\sigma\rangle\langle\sigma|_A \quad (\text{C40})$$

$$= K! \left( \frac{(d_A + K - 1)!}{(d_A - 1)!} \right)^{t-1} \left( \frac{(d_A d_B - 1)!}{(d_A d_B + K - 1)!} \right)^t, \quad (\text{C41})$$

and the  $K$ -th PS becomes

$$Z_{\text{HRCS}}^{(K)}(t) = \sum_{x(t), \mathbf{z}(t)} \mathbb{E}_{U \in \text{Haar}} [P_U[\mathbf{z}(t), x(t)]^K] = K! d_A d_B^t \left( \frac{(d_A + K - 1)!}{(d_A - 1)!} \right)^{t-1} \left( \frac{(d_A d_B - 1)!}{(d_A d_B + K - 1)!} \right)^t, \quad (\text{C42})$$

which completes the proof of Eq. (C28) in Theorem 8.

In the large system limit of  $d_A \gg 1$ , recall that the  $K$ -th PS for Haar random states is  $Z_{\text{H}}^{(K)}(N_{\text{eff}}) = K! (d_A d_B^t)! / (d_A d_B + K - 1)!$  (see Eq. (B21) with  $N = N_{\text{eff}} = N_A + tN_B$ ). The  $K$ -th PS ratio between Eq. (C28) of HRCS and Haar one becomes

$$\frac{Z_{\text{HRCS}}^{(K)}(t)}{Z_{\text{H}}^{(K)}(N_{\text{eff}})} = \frac{K! d_A d_B^t [(d_A + K - 1)!]^{t-1} [(d_A d_B - 1)!]^t (d_A d_B^t + K - 1)!}{[(d_A - 1)!]^{t-1} [(d_A d_B + K - 1)!]^t K! (d_A d_B^t)!} \quad (\text{C43})$$

$$= \frac{[(d_A + K - 1)!]^{t-1} [(d_A d_B - 1)!]^t (d_A d_B^t + K - 1)!}{[(d_A - 1)!]^{t-1} [(d_A d_B + K - 1)!]^t (d_A d_B^t - 1)!} \quad (\text{C44})$$

$$= \left[ \prod_{j=0}^{K-1} (d_A + j) \right]^{t-1} \left[ \prod_{j=0}^{K-1} (d_A d_B + j) \right]^{-t} \left[ \prod_{j=0}^{K-1} (d_A d_B^t + j) \right] \quad (\text{C45})$$

$$= \exp \left[ (t-1) \sum_{j=0}^{K-1} \log(d_A + j) - t \sum_{j=0}^{K-1} \log(d_A d_B + j) + \sum_{j=0}^{K-1} \log(d_A d_B^t + j) \right] \quad (\text{C46})$$

$$= \exp \left[ (t-1) \sum_{j=0}^{K-1} \left( \log(d_A) + \log \left( 1 + \frac{j}{d_A} \right) \right) - t \sum_{j=0}^{K-1} \left( \log(d_A d_B) + \log \left( 1 + \frac{j}{d_A d_B} \right) \right) \right. \\ \left. + \sum_{j=0}^{K-1} \left( \log(d_A d_B^t) \log \left( 1 + \frac{j}{d_A d_B^t} \right) \right) \right] \quad (\text{C47})$$

$$= \exp \left[ (t-1) \log(d_A) - t \log(d_A d_B) + \log(d_A d_B^t) \right] \\ \times \exp \left[ \sum_{j=0}^{K-1} \left( (t-1) \log \left( 1 + \frac{j}{d_A} \right) - t \log \left( 1 + \frac{j}{d_A d_B} \right) + \log \left( 1 + \frac{j}{d_A d_B^t} \right) \right) \right] \quad (\text{C48})$$

$$= \exp \left[ \sum_{j=0}^{K-1} \left( (t-1) \frac{j}{d_A} - t \frac{j}{d_A d_B} + \frac{j}{d_A d_B^t} \right) + \mathcal{O} \left( \frac{1}{d_A^2} \right) \right] \quad (\text{C49})$$

$$= \exp \left[ \frac{K(K-1)}{2d_A} \left( (t-1) - \frac{t}{d_B} + \frac{1}{d_B^t} \right) + \mathcal{O} \left( \frac{1}{d_A^2} \right) \right], \quad (\text{C50})$$

which is the asymptotic form in Eq. (C29). ■

For  $\epsilon$ -approximate  $K$ -th PS in HRCS defined by  $Z_{\text{HRCS}}^{(K)}(t) \leq (1 + \epsilon) Z_{\text{H}}^{(K)}(N_{\text{eff}})$ , similarly to the approach in CP, we again first introduce the upper bound to asymptotic form (Eq. (C29)) as

$$Z_{\text{HRCS}}^{(K)}(t) = Z_{\text{H}}^{(K)}(N_{\text{eff}}) \exp \left[ K(K-1) \frac{t(1 - d_B^{-1}) + d_B^{-t} - 1}{2d_A} + \mathcal{O} \left( \frac{1}{d_A^2} \right) \right] \\ \leq Z_{\text{H}}^{(K)}(N_{\text{eff}}) \exp \left[ K(K-1) \frac{t(1 - d_B^{-1}) - 1/2}{2d_A} + \mathcal{O} \left( \frac{1}{d_A^2} \right) \right]. \quad (\text{C51})$$

We instead require the upper bound above to satisfy the  $\epsilon$ -approximate PS and leads to

$$t \leq \tau^{(K)} \equiv \frac{d_B}{d_B - 1} \left( \frac{1}{2} + \frac{2d_A \log(1 + \epsilon)}{K(K-1)} \right), \quad (\text{C52})$$

which can also reduce to Eq. (C27) with  $K = 2$ .

### 3. Upper bound on total variation distance

In this section, we provide the proof to the upper bound on the total variation distance (TVD) in Methods. From the definition in Eq. (11), following the approach in Ref. [18], we have the upper bound by

$$\begin{aligned} \text{TVD} &= \mathbb{E}_C \mathbb{E}_U \left[ \frac{1}{2} \|P_C[\mathbf{y}] - P_U(\mathbf{y})\|_1 \right] \\ &\leq 2^{N_{\text{eff}}/2} \mathbb{E}_C \mathbb{E}_U \left[ \frac{1}{2} \|P_C(\mathbf{y}) - P_U(\mathbf{y})\|_2 \right] \end{aligned} \quad (\text{C53})$$

$$\leq \frac{1}{2} \sqrt{2^{N_{\text{eff}}} \mathbb{E}_C \mathbb{E}_U \|P_C(\mathbf{y}) - P_U(\mathbf{y})\|_2^2}, \quad (\text{C54})$$

where we denote  $\mathbf{y} = (\mathbf{z}, x)$  for simplicity.  $P_C[\mathbf{y}]$  is the sampling distribution in HRCS with circuit instance  $C$  and  $P_U[\mathbf{y}]$  is the sampling distribution from Haar random states with Haar unitary  $U$ . The expectation value

$$\begin{aligned} &\mathbb{E}_C \mathbb{E}_U \|P_C(\mathbf{y}) - P_U(\mathbf{y})\|_2^2 \\ &= \mathbb{E}_C \mathbb{E}_U \sum_{\mathbf{y}} P_C(\mathbf{y})^2 + P_U(\mathbf{y})^2 - 2P_C(\mathbf{y})P_U(\mathbf{y}) \end{aligned} \quad (\text{C55})$$

$$= Z_{\text{HRCS}}(t) + Z_{\text{H}}(N_{\text{eff}}) - 2 \sum_{\mathbf{y}} \mathbb{E}_C [P_C(\mathbf{y})] \mathbb{E}_U [P_U(\mathbf{y})] \quad (\text{C56})$$

$$= Z_{\text{HRCS}}(t) + Z_{\text{H}}(N_{\text{eff}}) - \frac{2^{N_{\text{eff}}+1}}{4^{N_{\text{eff}}}} \quad (\text{C57})$$

$$= Z_{\text{HRCS}}(t) - Z_{\text{H}}(N_{\text{eff}})/2^{N_{\text{eff}}}. \quad (\text{C58})$$

Inputting the above into Eq. (C54), we arrive at the upper bound for TVD

$$\text{TVD} \leq \frac{1}{2} \sqrt{2^{N_{\text{eff}}} Z_{\text{HRCS}}(t) - Z_{\text{H}}(N_{\text{eff}})} \quad (\text{C59})$$

$$\leq \frac{1}{2} \sqrt{2^{N_{\text{eff}}} Z_{\text{HRCS}}(t)} \quad (\text{C60})$$

$$\leq \frac{1}{2} \sqrt{2^{N_{\text{eff}}} Z_{\text{H}}(N_{\text{eff}}) \exp \left[ \frac{t-1}{d_A} + \mathcal{O} \left( \frac{1}{d_A^2} \right) \right]} \quad (\text{C61})$$

$$\leq \frac{1}{\sqrt{2}} \exp \left[ \frac{t-1}{2d_A} + \mathcal{O} \left( \frac{1}{d_A^2} \right) \right], \quad (\text{C62})$$

where we utilize Eq. (C25) to obtain leading order result.

### 4. Reset in HRCS

In this section, we show that whether adopting the reset strategy does not affect the CP and PS. The intuition is simple. Suppose we perform measurement on bath without following reset, we just need to add a few Pauli-X gate on corresponding bath qubits to flip their states from  $|1\rangle$  to  $|0\rangle$ . Since the circuit unitary is assumed to be Haar random and both CP and PS are defined to be ensemble-averaged over circuit unitaries, the result will not change. We present the detailed proof as follows.

The joint probability is

$$P'_U[\mathbf{z}(t), x(t)] = \text{tr} \left( U \left( |\mathbf{0}\rangle\langle\mathbf{0}|_A \otimes |\mathbf{0}\rangle\langle\mathbf{0}|_{B_0} \otimes \bigotimes_{j=1}^{t-1} |z_j\rangle\langle z_j|_{B_j} \right) U^\dagger |x(t)\rangle\langle x(t)|_A \otimes |\mathbf{z}(t)\rangle\langle\mathbf{z}(t)|_B \right) \quad (\text{C63})$$

$$= \text{tr} \left( U \left( |\mathbf{0}\rangle\langle\mathbf{0}|_A \otimes |\mathbf{0}\rangle\langle\mathbf{0}|_{B_0} \otimes \bigotimes_{j=1}^{t-1} X^{z_j} |\mathbf{0}\rangle\langle\mathbf{0}|_{B_j} X^{z_j} \right) U^\dagger |x(t)\rangle\langle x(t)|_A \otimes |\mathbf{z}(t)\rangle\langle\mathbf{z}(t)|_B \right) \quad (\text{C64})$$

$$= \text{tr} \left( U_{\mathbf{z}} \left( |\mathbf{0}\rangle\langle\mathbf{0}|_A \otimes |\mathbf{0}\rangle\langle\mathbf{0}|_{B_0} \otimes \bigotimes_{j=1}^{t-1} |\mathbf{0}\rangle\langle\mathbf{0}|_{B_j} \right) U_{\mathbf{z}}^\dagger |x(t)\rangle\langle x(t)|_A \otimes |\mathbf{z}(t)\rangle\langle\mathbf{z}(t)|_B \right), \quad (\text{C65})$$

where in last line we define  $U_{\mathbf{z}} = U_t X^{z_{t-1}} U_{t-1} \cdots X^{z_1} U_1$ . The ensemble-averaged CP then becomes

$$Z' = \mathbb{E}_{U \in \text{Haar}} \sum_{\mathbf{z}(t), x(t)} P_U[\mathbf{z}(t), x(t)]^2 \quad (\text{C66})$$

$$= \sum_{\mathbf{z}(t), x(t)} \mathbb{E}_{U \in \text{Haar}} \text{tr} \left( U_{\mathbf{z}} \left( |\mathbf{0}\rangle\langle\mathbf{0}|_A \otimes |\mathbf{0}\rangle\langle\mathbf{0}|_{B_0} \otimes_{j=1}^{t-1} |\mathbf{0}\rangle\langle\mathbf{0}|_{B_j} \right) U_{\mathbf{z}}^\dagger |x(t)\rangle\langle x(t)|_A \otimes |\mathbf{z}(t)\rangle\langle\mathbf{z}(t)|_{\mathbf{B}} \right) \quad (\text{C67})$$

$$= \sum_{\mathbf{z}(t), x(t)} \mathbb{E}_{V \in \text{Haar}} \text{tr} \left( V \left( |\mathbf{0}\rangle\langle\mathbf{0}|_A \otimes |\mathbf{0}\rangle\langle\mathbf{0}|_{B_0} \otimes_{j=1}^{t-1} |\mathbf{0}\rangle\langle\mathbf{0}|_{B_j} \right) V^\dagger |x(t)\rangle\langle x(t)|_A \otimes |\mathbf{z}(t)\rangle\langle\mathbf{z}(t)|_{\mathbf{B}} \right) \quad (\text{C68})$$

$$= Z, \quad (\text{C69})$$

where in the second to last line we utilize the left and right invariance property of Haar random unitaries. The proof for PS can be completed in the same way by replacing the exponent from 2 to  $K$ , and we don't repeat it here.

#### Appendix D: Marginal sampling in HRCS

In this section, we briefly present the theoretical results of spatial and temporal marginal sampling in HRCS, referring to the distribution of  $P[x(t)]$  and  $P[\mathbf{z}(t)]$ , both of which are near uniform in terms of CP.

The main results are the following, with detailed proofs in later sections.

**Theorem 9** *For holographic random circuit sampling with each unitary  $U_t$  satisfying 2-design, the ensemble-averaged collision probability for marginal spatial sampling with  $P[x(t)]$*

$$Z_{\text{Sp}}(t) = \frac{d_A d_B + 1}{d_A^2 d_B + 1} + \frac{(d_A - 1)(d_A d_B - 1)}{(d_A + 1)(d_A^2 d_B + 1)} \left( \frac{(d_A^2 - 1) d_B}{d_A^2 d_B^2 - 1} \right)^t \quad (\text{D1})$$

$$= Z_{\text{uni}}(N_A) \left( 1 + \frac{1}{d_A d_B} + \frac{1}{d_B^t} - \frac{2 + d_B^{-1}}{d_A d_B^t} \right) + \mathcal{O} \left( \frac{1}{d_A^3} \right), \quad (\text{D2})$$

where  $d_A, d_B = 2^{N_A}, 2^{N_B}$  are the Hilbert space dimensions of system and bath, and the second line holds for large system limit  $d_A \gg 1$ . For marginal temporal sampling with  $P[\mathbf{z}(t)]$ , we have

$$Z_{\text{Te}}(t) = \left( \frac{d_A + 1}{d_A d_B + 1} \right)^t \quad (\text{D3})$$

$$= Z_{\text{uni}}(t N_B) \exp \left[ \frac{t(d_B - 1)}{d_A d_B} + \mathcal{O} \left( \frac{1}{d_A^2} \right) \right]. \quad (\text{D4})$$

Firstly, a simple sanity check shows that at  $t = 1$ ,  $Z_{\text{Sp}}(t = 1) = (1 + d_B)/(1 + d_A d_B)$  and  $Z_{\text{Te}}(t = 1) = (1 + d_A)/(1 + d_A d_B)$ , which equals the CP of sampling only on the system or bath of Haar random states (see proof in Appendix B).

With increasing number of temporal steps  $t$ , the leading order approximation in Eq. (D2) indicates an exponential convergence of  $2^{-t N_B}$  toward the uniform distribution with a finite-size correction of  $1/d_A d_B$ . The convergence time-scale  $\sim 1/N_B$  follows the same scaling as the convergence toward first-order state design in holographic deep thermalization [28] and quantum information lifetime in unmonitored dynamics [29], determined by the dynamics of the average state of the system. For temporal sampling in HRCS, the asymptotic expression in Eq. (D4) indicates the convergence of CP toward the uniform one with a correction suppressed by  $d_A$ . The time-scale of convergence  $\sim d_A = 2^{N_A}$  is exponentially long. Despite the lack of AC, the CP of temporal sampling  $Z_{\text{Te}}(t)$  can serve as a benchmark for mid-circuit measurements.

We can also formally introduce  $\epsilon$ -approximate uniform distribution for both spatial and temporal sampling. For  $\epsilon$ -approximate uniform distribution with  $Z_{\text{Sp}}(t) \leq (1 + \epsilon) Z_{\text{uni}}(N_A)$ , we require the temporal steps to satisfy

$$t \geq \tau_{\text{Sp}} \equiv \log(1/\epsilon) / \log(2^{N_B}) + \mathcal{O}(2^{-N_A}). \quad (\text{D5})$$

The scaling  $\tau_{\text{Sp}} \sim 1/N_B$ .

For temporal sampling, when the number of temporal steps is upper limited by

$$t \leq \tau_{\text{Te}} \equiv 2^{N_A} \log(1 + \epsilon) \frac{2^{N_B}}{2^{N_B} - 1} \simeq 2^{N_A} \log(1 + \epsilon), \quad (\text{D6})$$

the temporal sampling distribution is  $\epsilon$ -approximate uniform distribution in CP  $Z_{\text{Te}} \leq (1 + \epsilon)Z_{\text{uni}}(tN_B)$ . Moreover, the approximation to uniform distribution within an exponential number of temporal steps provides evidence to support the generation of random states with nearly uniform probability in holographic deep thermalization [28]. On the other hand, beyond the critical time step  $\tau_{\text{Te}}$ , the CP grows exponentially with the number of steps, and the sampling distribution quickly becomes lack of AC.

### 1. Proof of Theorem 9

We will divide Theorem 9 into two parts, including the spatial part (Theorem 10) and temporal part (Theorem 11).

The proofs still rely on the equivalent expansion though with different boundary conditions (see Fig. 5b and c).

**Theorem 10** (*Theorem 9, spatial sampling part*) *For holographic random circuit sampling with each unitary  $U_t$  satisfying 2-design, the ensemble-averaged collision probability for marginal spatial sampling at step  $t \geq 1$  is*

$$Z_{\text{Sp}}(t) = \frac{d_A d_B + 1}{d_A^2 d_B + 1} + \frac{(d_A - 1)(d_A d_B - 1)}{(d_A + 1)(d_A^2 d_B + 1)} \left( \frac{(d_A^2 - 1) d_B}{d_A^2 d_B^2 - 1} \right)^t \quad (\text{D7})$$

$$= Z_{\text{uni}}(N_A) \left( 1 + \frac{1}{d_A d_B} + \frac{1}{d_B^t} - \frac{2 + d_B^{-1}}{d_A d_B^t} \right) + \mathcal{O}\left(\frac{1}{d_A^3}\right), \quad (\text{D8})$$

where  $d_A, d_B = 2^{N_A}, 2^{N_B}$  are the Hilbert space dimension of system and bath, and the second line holds for large system limit  $d_A \gg 1$ .

**Proof.** Following the equivalent expansion in Fig. 5b, we first write out the marginal probability of sampling  $x(t)$  in the output state as

$$P_U[x(t)] = \text{tr} (U |\mathbf{0}\rangle\langle\mathbf{0}|_{AB} U^\dagger |x(t)\rangle\langle x(t)|_A \otimes \mathbf{I}_B). \quad (\text{D9})$$

The ensemble average of the square of the marginal probability becomes

$$\mathbb{E}_{U \in \text{Haar}} [p_U[x(t)]^2] = \mathbb{E}_{U \in \text{Haar}} \text{tr} (U^{\otimes 2} |\mathbf{0}\rangle\langle\mathbf{0}|_{AB}^{\otimes 2} U^{\dagger \otimes 2} |x(t)\rangle\langle x(t)|_A^{\otimes 2} \otimes \mathbf{I}_B^{\otimes 2}) \quad (\text{D10})$$

$$= \langle\langle x(t) |_A \langle\langle \hat{e} |_B \mathbb{E}_{U \in \text{Haar}} [U^{\otimes 2} \otimes U^{*\otimes 2}] |\mathbf{0}\rangle\langle\mathbf{0}|_{AB}. \quad (\text{D11})$$

Now we evaluate Eq. (D11) step by step from  $U_1$  to  $U_t$ .

For the first step involving  $U_1$ , we have

$$\begin{aligned} & \langle\langle \hat{e} |_{B_1} \mathbb{E}_{U_1 \in \text{Haar}} [U_1^{\otimes 2} \otimes U_1^{*\otimes 2}] |\mathbf{0}\rangle\langle\mathbf{0}|_{AB_1} \\ &= \frac{1}{d^2 - 1} (\langle\langle \hat{e} | \hat{e} \rangle\langle \hat{e} |_{B_1} \langle\langle \hat{e} | \mathbf{0}\rangle\langle \mathbf{0}|_{AB_1} | \hat{e} \rangle\langle \hat{e}|_A + \langle\langle \hat{e} | \hat{\tau} \rangle\langle \hat{\tau} |_{B_1} \langle\langle \hat{\tau} | \mathbf{0}\rangle\langle \mathbf{0}|_{AB_1} | \hat{\tau} \rangle\langle \hat{\tau}|_A) \\ & \quad - \frac{1}{d(d^2 - 1)} (\langle\langle \hat{e} | \hat{e} \rangle\langle \hat{e} |_{B_1} \langle\langle \hat{\tau} | \mathbf{0}\rangle\langle \mathbf{0}|_{AB_1} | \hat{e} \rangle\langle \hat{e}|_A + \langle\langle \hat{e} | \hat{\tau} \rangle\langle \hat{\tau} |_{B_1} \langle\langle \hat{e} | \mathbf{0}\rangle\langle \mathbf{0}|_{AB_1} | \hat{\tau} \rangle\langle \hat{\tau}|_A) \end{aligned} \quad (\text{D12})$$

$$= \frac{1}{d^2 - 1} (d_B^2 | \hat{e} \rangle\langle \hat{e}|_A + d_B | \hat{\tau} \rangle\langle \hat{\tau}|_A) - \frac{1}{d(d^2 - 1)} (d_B^2 | \hat{e} \rangle\langle \hat{e}|_A + d_B | \hat{\tau} \rangle\langle \hat{\tau}|_A) \quad (\text{D13})$$

$$= \frac{d_B}{d_A(d_A d_B + 1)} | \hat{e} \rangle\langle \hat{e}|_A + \frac{1}{d_A(d_A d_B + 1)} | \hat{\tau} \rangle\langle \hat{\tau}|_A. \quad (\text{D14})$$

We next focus on the evolution of each of them separately under Haar random unitaries.

$$\begin{aligned} & \langle\langle \hat{e} |_{B_2} \mathbb{E}_{U_2 \in \text{Haar}} [U_2^{\otimes 2} \otimes U_2^{*\otimes 2}] | \hat{e} \rangle\langle \hat{e}|_A |\mathbf{0}\rangle\langle\mathbf{0}|_{B_2} \\ &= \frac{1}{d^2 - 1} (\langle\langle \hat{e} | \hat{e} \rangle\langle \hat{e} |_{B_2} \langle\langle \hat{e} | \mathbf{0}\rangle\langle \mathbf{0}|_{B_2} | \hat{e} \rangle\langle \hat{e}|_A + \langle\langle \hat{e} | \hat{\tau} \rangle\langle \hat{\tau} |_{B_2} \langle\langle \hat{\tau} | \hat{e} \rangle\langle \hat{e}|_A \langle\langle \hat{\tau} | \mathbf{0}\rangle\langle \mathbf{0}|_{B_2} | \hat{\tau} \rangle\langle \hat{\tau}|_A) \\ & \quad - \frac{1}{d(d^2 - 1)} (\langle\langle \hat{e} | \hat{e} \rangle\langle \hat{e} |_{B_2} \langle\langle \hat{\tau} | \hat{e} \rangle\langle \hat{e}|_A \langle\langle \hat{\tau} | \mathbf{0}\rangle\langle \mathbf{0}|_{B_2} | \hat{e} \rangle\langle \hat{e}|_A + \langle\langle \hat{e} | \hat{\tau} \rangle\langle \hat{\tau} |_{B_2} \langle\langle \hat{e} | \hat{e} \rangle\langle \hat{e}|_A \langle\langle \hat{\tau} | \mathbf{0}\rangle\langle \mathbf{0}|_{B_2} | \hat{\tau} \rangle\langle \hat{\tau}|_A) \end{aligned} \quad (\text{D15})$$

$$= \frac{1}{d^2 - 1} (d_A^2 d_B^2 | \hat{e} \rangle\langle \hat{e}|_A + d_A d_B | \hat{\tau} \rangle\langle \hat{\tau}|_A) - \frac{1}{d(d^2 - 1)} (d_A d_B^2 | \hat{e} \rangle\langle \hat{e}|_A + d_A^2 d_B | \hat{\tau} \rangle\langle \hat{\tau}|_A) \quad (\text{D16})$$

$$= \frac{d_B (d_A^2 d_B - 1)}{d_A^2 d_B^2 - 1} | \hat{e} \rangle\langle \hat{e}|_A + \frac{d_A (d_B - 1)}{d_A^2 d_B^2 - 1} | \hat{\tau} \rangle\langle \hat{\tau}|_A. \quad (\text{D17})$$

Similarly, for  $\tau$ , we have

$$\begin{aligned} & \langle\langle \hat{e} | \rangle\rangle_{B_2} \mathbb{E}_{U_2 \in \text{Haar}} [U_2^{\otimes 2} \otimes U_2^{*\otimes 2}] |\hat{\tau}\rangle\rangle_A |\mathbf{0}\rangle\rangle_{B_2} \\ &= \frac{1}{d^2 - 1} (\langle\langle \hat{e} | \hat{e} \rangle\rangle_{B_2} \langle\langle \hat{e} | \hat{\tau} \rangle\rangle_A \langle\langle \hat{e} | \mathbf{0} \rangle\rangle_{B_2} |\hat{e}\rangle\rangle_A + \langle\langle \hat{e} | \hat{\tau} \rangle\rangle_{B_2} \langle\langle \hat{\tau} | \hat{\tau} \rangle\rangle_A \langle\langle \hat{\tau} | \mathbf{0} \rangle\rangle_{B_2} |\hat{\tau}\rangle\rangle_A) \\ &\quad - \frac{1}{d(d^2 - 1)} (\langle\langle \hat{e} | \hat{e} \rangle\rangle_{B_2} \langle\langle \hat{\tau} | \hat{\tau} \rangle\rangle_A \langle\langle \hat{\tau} | \mathbf{0} \rangle\rangle_{B_2} |\hat{e}\rangle\rangle_A + \langle\langle \hat{e} | \hat{\tau} \rangle\rangle_{B_2} \langle\langle \hat{e} | \hat{\tau} \rangle\rangle_A \langle\langle \hat{e} | \mathbf{0} \rangle\rangle_{B_2} |\hat{\tau}\rangle\rangle_A) \end{aligned} \quad (\text{D18})$$

$$= \frac{1}{d^2 - 1} (d_A d_B^2 |\hat{e}\rangle\rangle_A + d_A^2 d_B |\hat{\tau}\rangle\rangle_A) - \frac{1}{d(d^2 - 1)} (d_A^2 d_B^2 |\hat{e}\rangle\rangle_A + d_A d_B |\hat{\tau}\rangle\rangle_A) \quad (\text{D19})$$

$$= \frac{d_A d_B (d_B - 1)}{d_A^2 d_B^2 - 1} |\hat{e}\rangle\rangle_A + \frac{d_A^2 d_B - 1}{d_A^2 d_B^2 - 1} |\hat{\tau}\rangle\rangle_A. \quad (\text{D20})$$

We still utilize the 2-dimensional linear system representation as  $|\underline{0}\rangle \equiv |\hat{e}\rangle\rangle_A, |\underline{1}\rangle \equiv |\hat{\tau}\rangle\rangle_A$ . The mapping in Eq. (D17) and Eq. (D20) can be represented by a  $2 \times 2$  matrix as

$$M_2 = \frac{1}{d_A^2 d_B^2 - 1} \begin{pmatrix} d_B (d_A^2 d_B - 1) & d_A d_B (d_B - 1) \\ d_A (d_B - 1) & d_A^2 d_B - 1 \end{pmatrix}, \quad (\text{D21})$$

and the ensemble-averaged squared probability in Eq. (D11) becomes

$$\mathbb{E}_{U \in \text{Haar}} [P_U[x(t)]^2] = \frac{d_B}{d_A(d_A d_B + 1)} (\langle \underline{0} | + \langle \underline{1} |) M_2^{t-1} |\underline{0}\rangle + \frac{1}{d_A(d_A d_B + 1)} (\langle \underline{0} | + \langle \underline{1} |) M_2^{t-1} |\underline{1}\rangle \quad (\text{D22})$$

$$= \frac{d_A d_B + 1}{d_A (d_A^2 d_B + 1)} + \frac{(d_A - 1)(d_A d_B - 1)}{d_A(d_A + 1)(d_A^2 d_B + 1)} \left( \frac{(d_A^2 - 1) d_B}{d_A^2 d_B^2 - 1} \right)^t. \quad (\text{D23})$$

Therefore, the ensemble-averaged CP is

$$Z_{\text{Sp}}(t) = \sum_{x(t)} \mathbb{E}_{U \in \text{Haar}} [P_U[x(t)]^2] \quad (\text{D24})$$

$$= \frac{d_A d_B + 1}{d_A^2 d_B + 1} + \frac{(d_A - 1)(d_A d_B - 1)}{(d_A + 1)(d_A^2 d_B + 1)} \left( \frac{(d_A^2 - 1) d_B}{d_A^2 d_B^2 - 1} \right)^t, \quad (\text{D25})$$

which proves Eq. (D7) in Theorem 10. In the large system limit of  $d_A \gg 1$ , we can directly have the asymptotic form in Eq. (D8) with  $Z_{\text{uni}}(N_A) = 2^{-N_A}$  to be the CP for uniform distribution. ■

For the  $\epsilon$ -approximate uniform CP of spatial marginal sampling in HRCS, defined by  $Z_{\text{Sp}}(t) \leq (1 + \epsilon) Z_{\text{uni}}(N_A)$ . As  $Z_{\text{Sp}}(t)$  monotonically decays with  $t$ , we introduce an upper bound for simplification

$$\begin{aligned} Z_{\text{Sp}}(t) &= Z_{\text{uni}}(N_A) \left( 1 + \frac{1}{d_A d_B} + \frac{1}{d_B^t} - \frac{2 + d_B^{-1}}{d_A d_B^t} \right) + \mathcal{O}\left(\frac{1}{d_A^3}\right) \\ &\leq Z_{\text{uni}}(N_A) \left( 1 + \frac{1}{d_A d_B} + \frac{1}{d_B^t} \right) + \mathcal{O}\left(\frac{1}{d_A^3}\right), \end{aligned} \quad (\text{D26})$$

which results in the critical number of temporal steps as

$$t \geq \tau_{\text{Sp}} \equiv \frac{\log\left(\frac{d_A d_B}{d_A d_B \epsilon - 1}\right)}{\log(d_B)} = \frac{\log(1/\epsilon) + \mathcal{O}(1/d_A)}{\log(d_B)}. \quad (\text{D27})$$

**Theorem 11** (Theorem 9, temporal sampling part) *For holographic random circuit sampling with each unitary  $U_t$  satisfying 2-design, the ensemble-averaged collision probability for marginal temporal sampling at step  $t \geq 1$  is*

$$Z_{\text{Te}}(t) = \left( \frac{d_A + 1}{d_A d_B + 1} \right)^t, \quad (\text{D28})$$

where  $d_A = 2^{N_A}, d_B = 2^{N_B}$  are Hilbert space dimensions of system and bath. In the large system limit of  $d_A \gg 1$ , we have

$$Z_{\text{Te}}(t) = Z_{\text{uni}}(t N_B) \exp \left[ \frac{t(d_B - 1)}{d_A d_B} + \mathcal{O}\left(\frac{1}{d_A^2}\right) \right]. \quad (\text{D29})$$

**Proof.** As illustrated by the bath expansion in Fig. 5c, the marginal probability of sampling  $\mathbf{z}(t)$  in the output state

$$P_U[\mathbf{z}(t)] = \text{tr} (U |\mathbf{0}\rangle\langle\mathbf{0}|_{AB} U^\dagger \mathbf{I}_A \otimes |\mathbf{z}(t)\rangle\langle\mathbf{z}(t)|_B), \quad (\text{D30})$$

where  $\mathbf{z}(t) = (z_1, z_2, \dots, z_t)$ . The ensemble average of the square of the marginal probability becomes

$$\mathbb{E}_{U \in \text{Haar}} [P_U[\mathbf{z}(t)]^2] = \mathbb{E}_{U \in \text{Haar}} \text{tr} (U^{\otimes 2} |\mathbf{0}\rangle\langle\mathbf{0}|_{AB}^{\otimes 2} U^{\dagger \otimes 2} \mathbf{I}_A^{\otimes 2} |\mathbf{z}(t)\rangle\langle\mathbf{z}(t)|_B^{\otimes 2}) \quad (\text{D31})$$

$$= \langle\langle \hat{e} |_A \langle\langle \mathbf{z}(t) |_B \mathbb{E}_{U \in \text{Haar}} [U^{\otimes 2} \otimes U^{*\otimes 2}] |\mathbf{0}\rangle\langle\mathbf{0}|_{AB} \rangle\langle\langle \hat{e} |_A \langle\langle \mathbf{z}(t) |_B \quad (\text{D32})$$

Now we evaluate Eq. (D32) step by step from  $U_1$  to  $U_t$ .

For the first step involving  $U_1$ , we have

$$\langle\langle z_1 |_{B_1} \mathbb{E}_{U_1 \in \text{Haar}} [U_1^{\otimes 2} \otimes U_1^{*\otimes 2}] |\mathbf{0}\rangle\langle\mathbf{0}|_{AB_1} = \frac{1}{d(d+1)} (|\hat{e}\rangle\langle\hat{e}|_A + |\hat{\tau}\rangle\langle\hat{\tau}|_A), \quad (\text{D33})$$

which is already derived in Eq. (C8). We next focus on the evolution of each of them separately under Haar random unitary (see derivation in Eqs. (C11), (C14)).

$$\begin{cases} \langle\langle z_2 |_{B_2} \mathbb{E}_{U_2 \in \text{Haar}} [U_2^{\otimes 2} \otimes U_2^{*\otimes 2}] |\hat{e}\rangle\langle\hat{e}|_A |\mathbf{0}\rangle\langle\mathbf{0}|_{B_2} = \frac{d_A^2 d_B - 1}{d_B(d_A^2 d_B^2 - 1)} |\hat{e}\rangle\langle\hat{e}|_A + \frac{d_A(d_B - 1)}{d_B(d_A^2 d_B^2 - 1)} |\hat{\tau}\rangle\langle\hat{\tau}|_A, \\ \langle\langle z_2 |_{B_2} \mathbb{E}_{U_2 \in \text{Haar}} [U_2^{\otimes 2} \otimes U_2^{*\otimes 2}] |\hat{\tau}\rangle\langle\hat{\tau}|_A |\mathbf{0}\rangle\langle\mathbf{0}|_{B_2} = \frac{d_A(d_B - 1)}{d_B(d_A^2 d_B^2 - 1)} |\hat{e}\rangle\langle\hat{e}|_A + \frac{d_A^2 d_B - 1}{d_B(d_A^2 d_B^2 - 1)} |\hat{\tau}\rangle\langle\hat{\tau}|_A. \end{cases} \quad (\text{D34})$$

With the 2-dimensional linear system representation as  $|\underline{0}\rangle \equiv |\hat{e}\rangle_A, |\underline{1}\rangle \equiv |\hat{\tau}\rangle_A$ , the mapping of Eqs. (D34) can be represented by the  $2 \times 2$  matrix in Eq. (C15) and the ensemble-averaged squared probability in Eq. (D11) becomes

$$\mathbb{E}_{U \in \text{Haar}} [P_U[\mathbf{z}(t)]^2] = \frac{1}{d(d+1)} [|\underline{0}\rangle M^{t-1} (|\underline{0}\rangle + |\underline{1}\rangle) \langle\langle \hat{e} | \hat{e} \rangle\langle\langle \hat{e} | + |\underline{1}\rangle M^{t-1} (|\underline{0}\rangle + |\underline{1}\rangle) \langle\langle \hat{e} | \hat{\tau} \rangle\langle\langle \hat{\tau} |] \quad (\text{D35})$$

$$= \left( \frac{1 + d_A}{d_B(1 + d_A d_B)} \right)^t. \quad (\text{D36})$$

Therefore, the ensemble-averaged CP is

$$Z_{\text{Te}}(t) = \sum_{\mathbf{z}(t)} \mathbb{E}_{U \in \text{Haar}} [P_U[\mathbf{z}(t)]^2] = \left( \frac{1 + d_A}{1 + d_A d_B} \right)^t, \quad (\text{D37})$$

which proves Eq. (D28) in Theorem 11.

In the large system limit of  $d_A \gg 1$ , we have

$$\begin{aligned} Z_{\text{Te}}(t) &= \left( \frac{1 + d_A}{1 + d_A d_B} \right)^t \\ &= \exp \left[ t \log \left( \frac{1 + d_A}{1 + d_A d_B} \right) \right] \end{aligned} \quad (\text{D38})$$

$$= \exp \left[ t \log \left( \frac{1}{d_B} \right) + t \left( \frac{d_B - 1}{d_A d_B} \right) + \mathcal{O} \left( \frac{1}{d_A^2} \right) \right] \quad (\text{D39})$$

$$= Z_{\text{uni}}(t N_B) \exp \left[ t \left( \frac{d_B - 1}{d_A d_B} \right) + \mathcal{O} \left( \frac{1}{d_A^2} \right) \right], \quad (\text{D40})$$

which is the asymptotic result in Eq. (D29). ■

For  $\epsilon$ -approximate uniform CP defined by  $Z_{\text{Te}}(t) \leq (1 + \epsilon) Z_{\text{uni}}(t N_B)$ , we require

$$t \leq \tau_{\text{Te}} \equiv \frac{d_B}{d_B - 1} d_A \log(1 + \epsilon). \quad (\text{D41})$$

## 2. Temporal sampling per step in HRCS

In this section, we focus on the marginal temporal sampling per step in HRCS, i.e., the distribution of  $P[z_1], P[z_2], \dots, P[z_t]$ , and we derive a theoretical result with respect to AC as follows.

**Theorem 12** (Temporal sampling per step in HRCS) *For holographic random circuit sampling with each unitary  $U_t$  satisfying 2-design, the ensemble-averaged collision probability for temporal sampling only at a single step  $t \geq 1$  is*

$$Z_{\text{Te},t}(t) = \frac{d_A^2 + 1}{d_A^2 d_B + 1} + \frac{d_A(d_B - 1)(d_A d_B - 1)}{(d_A^2 d_B + 1)(d_A + 1)d_B} \left( \frac{(d_A^2 - 1)d_B}{d_A^2 d_B^2 - 1} \right)^t, \quad (\text{D42})$$

where  $d_A, d_B = 2^{N_A}, 2^{N_B}$  are the Hilbert space dimension of memory and bath system. In the large-system limit with  $d_A \gg 1$ , we have

$$Z_{\text{Te},t}(t) = Z_{\text{uni}}(N_B) \left( 1 + \frac{1 - d_B^{-1}}{d_A^2} + \frac{1}{d_A d_B^{t-1}} \left( 1 - \frac{1}{d_A} - \frac{1}{d_B} + \frac{1}{d_A d_B^2} \right) \right) + \mathcal{O} \left( \frac{1}{d_A^3} \right). \quad (\text{D43})$$

Note that the CP only depends on the step index  $t$  but independent of the total number of steps in HRCS as expected.

**Proof.** We prove it utilizing the expansion shown in Fig. 5d. Without loosing generality, we focus on the marginal temporal sampling only at step  $t$  assuming there are in total  $T$  steps in HRCS, and the sampling probability thus becomes

$$P_U[z_t] = \text{tr} \left( U |\mathbf{0}\rangle\langle\mathbf{0}|_{AB} U^\dagger \mathbf{I}_A \otimes \mathbf{I}_{B_1 \rightarrow B_{t-1}} \otimes |z_t\rangle\langle z_t|_{B_t} \otimes \mathbf{I}_{B_{t+1} \rightarrow B_T} \right), \quad (\text{D44})$$

where  $\mathbf{I}_{B_1 \rightarrow B_{t-1}} = \otimes_{j=1}^{t-1} \mathbf{I}_{B_j}$  and  $\mathbf{I}_{B_{t+1} \rightarrow B_T}$  is defined similarly. The ensemble-averaged squared probability becomes

$$\mathbb{E}_{U \in \text{Haar}} [P_U[z_t]^2] = \mathbb{E}_{U \in \text{Haar}} \text{tr} \left( U^{\otimes 2} |\mathbf{0}\rangle\langle\mathbf{0}|_{AB}^{\otimes 2} U^{\dagger \otimes 2} \mathbf{I}_A^{\otimes 2} \otimes \mathbf{I}_{B_1 \rightarrow B_{t-1}}^{\otimes 2} \otimes |z_t\rangle\langle z_t|_{B_t}^{\otimes 2} \otimes \mathbf{I}_{B_{t+1} \rightarrow B_T}^{\otimes 2} \right) \quad (\text{D45})$$

$$= \langle\langle \hat{e} |_{B_1 \rightarrow B_{t-1}} \langle\langle \hat{e} |_{B_t} \langle\langle z_t |_{B_t} \langle\langle \hat{e} |_{B_{t+1} \rightarrow B_T} \mathbb{E}_{U \in \text{Haar}} [U^{\otimes 2} \otimes U^{*\otimes 2}] |\mathbf{0}\rangle_{AB}, \quad (\text{D46})$$

where  $|\hat{e}\rangle\langle\hat{e}|_{B_1 \rightarrow B_{t-1}} = \otimes_{j=1}^{t-1} |\hat{e}\rangle\langle\hat{e}|_{B_j}$ .

For the first step unitary twirling with  $U_1$ , we have

$$\langle\langle \hat{e} |_{B_1} \mathbb{E}_{U_1 \in \text{Haar}} [U_1^{\otimes 2} \otimes U_1^{*\otimes 2}] |\mathbf{0}\rangle_{AB_1} = \frac{d_B}{d_A(d_A d_B + 1)} |\hat{e}\rangle\langle\hat{e}|_A + \frac{1}{d_A(d_A d_B + 1)} |\hat{\tau}\rangle\langle\hat{\tau}|_A, \quad (\text{D47})$$

which has been derived in Eq. (D14). The unitary twirling for  $|\hat{e}\rangle\langle\hat{e}|$  and  $|\hat{\tau}\rangle\langle\hat{\tau}|$  are

$$\begin{cases} \langle\langle \hat{e} |_{B_2} \mathbb{E}_{U_2 \in \text{Haar}} [U_2^{\otimes 2} \otimes U_2^{*\otimes 2}] |\hat{e}\rangle\langle\hat{e}|_A |\mathbf{0}\rangle_{B_2} &= \frac{d_B(d_A^2 d_B - 1)}{d_A^2 d_B^2 - 1} |\hat{e}\rangle\langle\hat{e}|_A + \frac{d_A(d_B - 1)}{d_A^2 d_B^2 - 1} |\hat{\tau}\rangle\langle\hat{\tau}|_A, \\ \langle\langle \hat{e} |_{B_2} \mathbb{E}_{U_2 \in \text{Haar}} [U_2^{\otimes 2} \otimes U_2^{*\otimes 2}] |\hat{\tau}\rangle\langle\hat{\tau}|_A |\mathbf{0}\rangle_{B_2} &= \frac{d_A d_B(d_B - 1)}{d_A^2 d_B^2 - 1} |\hat{e}\rangle\langle\hat{e}|_A + \frac{d_A^2 d_B - 1}{d_A^2 d_B^2 - 1} |\hat{\tau}\rangle\langle\hat{\tau}|_A. \end{cases} \quad (\text{D48})$$

Note that the above twirling result can be represented by  $M_2$  in Eq. (D21). Through the first  $t-1$  steps of evolution, we reach

$$\begin{aligned} & \mathbb{E}_{U \in \text{Haar}} \text{tr}_{B_1 \rightarrow B_{t-1}} \left( U_{1 \rightarrow t-1}^{\otimes 2} |\mathbf{0}\rangle\langle\mathbf{0}|_{A, B_1 \rightarrow B_{t-1}}^{\otimes 2} U_{1 \rightarrow t-1}^{\dagger \otimes 2} \mathbf{I}_{B_1 \rightarrow B_{t-1}}^{\otimes 2} \right) \\ &= \left( \frac{d_B}{d_A(d_A d_B + 1)} \langle 0 | M_2^{t-2} | 0 \rangle + \frac{1}{d_A(d_A d_B + 1)} \langle 0 | M_2^{t-2} | 1 \rangle \right) |\hat{e}\rangle\langle\hat{e}|_A \\ &+ \left( \frac{d_B}{d_A(d_A d_B + 1)} \langle 1 | M_2^{t-2} | 0 \rangle + \frac{1}{d_A(d_A d_B + 1)} \langle 1 | M_2^{t-2} | 1 \rangle \right) |\hat{\tau}\rangle\langle\hat{\tau}|_A \end{aligned} \quad (\text{D49})$$

$$\begin{aligned} &= \left[ \frac{d_B}{d_A^2 d_B + 1} - \frac{(d_A d_B - 1)^2 (d_A d_B + 1) \left( \frac{(d_A^2 - 1)d_B}{d_A^2 d_B^2 - 1} \right)^t}{d_A d_B (d_A - 1) (d_A + 1)^2 (d_A^2 d_B + 1)} \right] |\hat{e}\rangle\langle\hat{e}|_A \\ &+ \left[ \frac{1}{d_A (d_A^2 d_B + 1)} + \frac{(d_A d_B - 1)^2 (d_A d_B + 1) \left( \frac{(d_A^2 - 1)d_B}{d_A^2 d_B^2 - 1} \right)^t}{(d_A - 1) (d_A + 1)^2 d_B (d_A^2 d_B + 1)} \right] |\hat{\tau}\rangle\langle\hat{\tau}|_A. \end{aligned} \quad (\text{D50})$$

Next we do the unitary twirling with  $U_t$  for different boundary condition.

$$\begin{cases} \langle\langle z_t |_{B_t} \mathbb{E}_{U_t \in \text{Haar}} [U_t^{\otimes t} \otimes U_t^{*\otimes 2}] |\hat{e}\rangle\rangle_A |\mathbf{0}\rangle\rangle_{B_t} = \frac{d_A^2 d_B - 1}{d_B(d_A^2 d_B^2 - 1)} |\hat{e}\rangle\rangle_A + \frac{d_A(d_B - 1)}{d_B(d_A^2 d_B^2 - 1)} |\hat{\tau}\rangle\rangle_A, \\ \langle\langle z_t |_{B_t} \mathbb{E}_{U_t \in \text{Haar}} [U_t^{\otimes 2} \otimes U_t^{*\otimes 2}] |\hat{\tau}\rangle\rangle_A |\mathbf{0}\rangle\rangle_{B_t} = \frac{d_A(d_B - 1)}{d_B(d_A^2 d_B^2 - 1)} |\hat{e}\rangle\rangle_A + \frac{d_A^2 d_B - 1}{d_B(d_A^2 d_B^2 - 1)} |\hat{\tau}\rangle\rangle_A, \end{cases} \quad (\text{D51})$$

which is the same as Eqs. (D34). Applying it to Eq. (D50), we have

$$\begin{aligned} & \mathbb{E}_{U \in \text{Haar}} \text{tr}_{B_{1 \rightarrow t}} \left( U_{1 \rightarrow t}^{\otimes 2} |\mathbf{0}\rangle\langle \mathbf{0}|_{A, B_{1 \rightarrow t}}^{\otimes 2} U_{1 \rightarrow t}^{\dagger \otimes 2} \mathbf{I}_{B_{1 \rightarrow t}}^{\otimes 2} \right) \\ &= \frac{(1 - d_A d_B) \left( \frac{(d_A^2 - 1) d_B}{d_A^2 d_B^2 - 1} \right)^t + d_A(d_A + 1) d_B}{d_A(d_A + 1) d_B^2 (d_A^2 d_B + 1)} |\hat{e}\rangle\rangle_A + \frac{d_A(d_A d_B - 1) \left( \frac{(d_A^2 - 1) d_B}{d_A^2 d_B^2 - 1} \right)^t + d_A + 1}{d_A(d_A + 1) d_B (d_A^2 d_B + 1)} |\hat{\tau}\rangle\rangle_A. \end{aligned} \quad (\text{D52})$$

The following unitary twirling from  $U_{t+1}$  to  $U_T$  is still described by Eq. (D48), and we can finally derive the full expression of Eq. (D46) as

$$\mathbb{E}_{U \in \text{Haar}} [P_U[z_t]^2] = \frac{d_A(d_B - 1)(d_A d_B - 1)}{d_B^2 (d_A + 1)(d_A^2 d_B + 1)} \left( \frac{(d_A^2 - 1) d_B}{d_A^2 d_B^2 - 1} \right)^t + \frac{d_A^2 + 1}{d_B(d_A^2 d_B + 1)}, \quad (\text{D53})$$

and the CP becomes

$$Z_{\text{Te},t}(t) = \sum_{z_t} \mathbb{E}_{U \in \text{Haar}} [P_U[z_t]^2] = \frac{d_A(d_B - 1)(d_A d_B - 1)}{d_B(d_A + 1)(d_A^2 d_B + 1)} \left( \frac{(d_A^2 - 1) d_B}{d_A^2 d_B^2 - 1} \right)^t + \frac{d_A^2 + 1}{d_A^2 d_B + 1}. \quad (\text{D54})$$

■ Moreover, when the temporal step  $t$  satisfies

$$t \geq \tau_{\text{Te},t} \equiv \frac{\log \left( \frac{(d_B - 1)(d_A d_B - d_B - 1)}{d_A^2 d_B - d_B + 1} \right)}{\log(d_B)} = \frac{\log \left( \frac{d_B - 1}{d_A \epsilon} \right) + \mathcal{O} \left( \frac{1}{d_A} \right)}{\log(d_B)}, \quad (\text{D55})$$

the corresponding measurement statistics can be regarded as  $\epsilon$ -approximate uniform CP. Note that we have  $\tau_{\text{Te},t} \sim 1/N_B$ , which coincides with the scaling in spatial sampling of Eq. (D27) and aligns with the quantum information lifetime in the unmonitored dynamics identified in Ref. [29].

### 3. Additional numerical results on marginal sampling in HRCS

We verify the decay of CP in spatial sampling in Fig. 6a. Specifically, the relative deviation of CP with respect to uniform one  $Z_{\text{Sp}}(t)/Z_{\text{uni}}(N_A) - 1$  reveals an exponential decay in early stage of  $2^{-tN_B}$  (dashed lines) and later convergence to the finite-size correction of  $1/d_A^2 d_B$ . The critical temporal steps for  $\epsilon$ -approximate uniform CP in Eq. (D5) aligns with the numerical solutions (crosses) in Fig. 6b. Moreover, we plot the PoP of marginal spatial sampling distribution  $P[x(t)]$  in Fig. 6c, which concentrates around the uniform distribution with probability  $2^{-N_A}$ . Similar to the spatial sampling, we also see agreements between numerical results and theories for temporal sampling in Fig. 6d-e. The PoP of marginal temporal sampling  $P[\mathbf{z}(t)]$  also concentrates around the uniform distribution of dimension  $tN_B$  though with finite spreading.

### Appendix E: Noisy theory of XEB fidelity in HRCS

In this section, we introduce and derive the XEB fidelity dynamics of HRCS in the presence of noise. To model the circuit noise in the HRCS, we add a local depolarizing channel  $\mathcal{N}(\cdot)$  to the system  $A$  and bath  $B$  simultaneously following the circuit unitary  $U_t$  in each step, as shown in Fig. 7 top. Here, we consider the depolarizing channel on a  $d$ -dimensional system as

$$\mathcal{N}(\rho) = \gamma \rho + (1 - \gamma) \mathbf{I}/d, \quad (\text{E1})$$

where  $\mathbf{I}/d$  is the fully mixed state of dimension  $d$  and  $1 - \gamma$  is depolarizing probability. As  $\gamma$  is a free parameter, for simplicity of theoretical analysis, we assume that the noise parameter  $\gamma$  for the depolarizing channel in our noisy

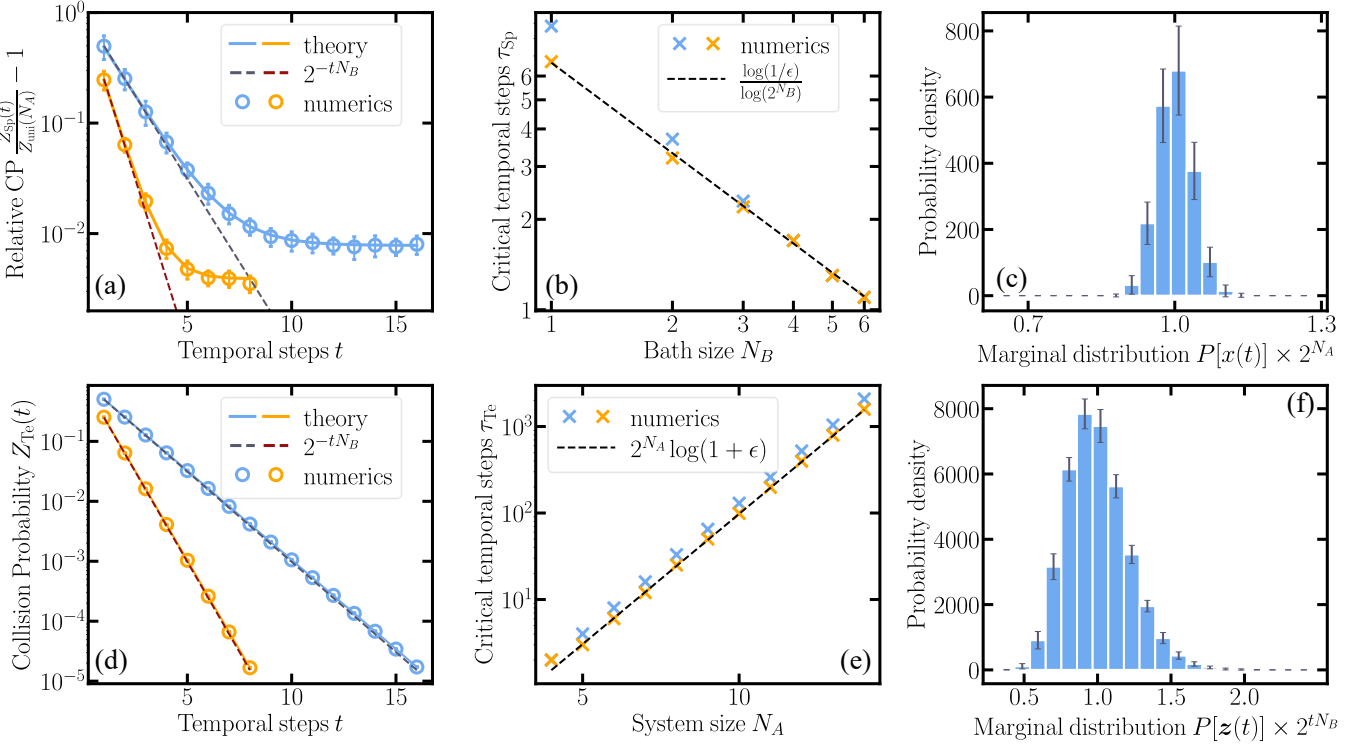


Figure 6. **Marginal sampling in HRCS.** (a) Ensemble-averaged relative deviation of collision probability (CP)  $Z_{Sp}(t)/Z_{uni}(N_A) - 1$  for spatial sampling in HRCS versus temporal steps in a system of  $N_A = 6, N_B = 1, 2$  (blue and orange dots) qubits. Light-colored solid lines represent theoretical result from Eq. (D1) in Theorem 9. Dark-colored dashed lines are universal convergence scaling of  $2^{-tN_B}$ . (b) Growth of critical temporal steps  $\tau_{Sp}$  versus bath size  $N_B$ . Blue and orange crosses represent numerical solutions for  $Z_{Sp}(t) = (1 + \epsilon)Z_{uni}(N_A)$  for  $N_A = 6, 12$  separately. The black line is Eq. (D5). (c) Ensemble-averaged probability density function of the spatial sampling distribution  $P[x(t)]$  in HRCS of  $N_A = 6, N_B = 4$  qubits at  $t = 3$ . (d) CP of temporal sampling  $Z_{Te}(t)$  versus temporal steps  $t$ . Light-colored solid lines are theory corresponding to Eq. (D3) in Theorem 9 and dark-colored dashed lines are CP for uniform distribution  $Z_{uni}(tN_B)$ . (e) Critical temporal steps for temporal sampling  $\tau_{Te}$  versus system size  $N_A$ . Blue and orange crosses represent numerical solutions for  $Z_{Te}(t) = (1 + \epsilon)Z_{uni}(tN_B)$  for  $N_B = 2, 6$  separately. The black line is Eq. (D6). (f) Ensemble-averaged probability density function of the temporal sampling distribution  $P[z(t)]$  in HRCS of  $N_A = 6, N_B = 4$  qubits at  $t = 3$ . Error bars in (a), (c), (d), (f) show the standard deviation over 50 circuit instances.

circuit model is a constant, independent of time  $t$  and the choice of system  $A$  or bath  $B$ . In practice, the circuit noise could be more complicated and the noise level can depend on number of qubits as well as time drift.

Similar to the noiseless derivation in Appendix C, we still expand the bath system in different steps,  $B_1, B_2, \dots, B_t$ , to an equivalent joint bath system  $\mathbf{B} = (B_1, B_2, \dots, B_t)$ , shown in Fig. 7 bottom. Therefore, we can write out the noisy sampling probability of  $\mathbf{z}(t), x(t)$  as

$$\tilde{P}[\mathbf{z}(t), x(t)] = \text{tr} \left( \tilde{\mathcal{U}} [|\mathbf{0}\rangle\langle\mathbf{0}|_{AB}] |x(t), \mathbf{z}(t)\rangle\langle x(t), \mathbf{z}(t)|_{AB} \right), \quad (\text{E2})$$

where  $\tilde{\mathcal{U}}$  represents the noisy circuit channel, explicitly defined as

$$\tilde{\mathcal{U}} \equiv (\mathcal{N}_{AB_t} \circ \mathcal{U}_t) \circ \dots \circ (\mathcal{N}_{AB_1} \circ \mathcal{U}_1), \quad (\text{E3})$$

with  $\mathcal{U}_t(\cdot) \equiv U_t(\cdot)U_t^\dagger$  to be noiseless unitary channel. Here,  $\mathcal{N}_{AB_t} = \mathcal{N}_A \otimes \mathcal{N}_{B_t}$  is a composite of local channels on  $A$  and  $B_t$  with each channel following Eq. (E1). Recall that the XEB fidelity in noisy circuit becomes

$$\tilde{\mathcal{F}}_{\text{XEB}}(t) = 2^{N_{\text{eff}}(t)} \left( \sum_{\mathbf{z}(t), x(t)} P[\mathbf{z}(t), x(t)] \tilde{P}[\mathbf{z}(t), x(t)] \right) - 1, \quad (\text{E4})$$

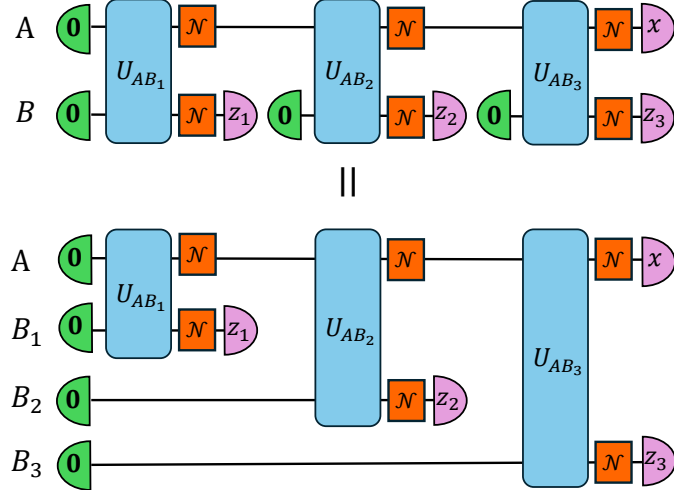


Figure 7. Circuit diagram for the expansion of bath system in noisy HRCS. Here we show an example of  $t = 3$  steps.

we evaluate the probability product as follows.

$$P[\mathbf{z}(t), x(t)] \tilde{P}[\mathbf{z}(t), x(t)] = \text{tr}(\mathcal{U}[\mathbf{0}\langle\mathbf{0}|_{AB}] |x(t), \mathbf{z}(t)\rangle\langle x(t), \mathbf{z}(t)|_{AB}) \text{tr}(\tilde{\mathcal{U}}[\mathbf{0}\langle\mathbf{0}|_{AB}] |x(t), \mathbf{z}(t)\rangle\langle x(t), \mathbf{z}(t)|_{AB}) \quad (\text{E5})$$

$$= \text{tr} \left[ (\mathcal{U} \otimes \tilde{\mathcal{U}}) \left[ |\mathbf{0}\langle\mathbf{0}|_{AB}^{\otimes 2} \right] |x(t), \mathbf{z}(t)\rangle\langle x(t), \mathbf{z}(t)|_{AB}^{\otimes 2} \right] \quad (\text{E6})$$

$$= \text{tr} \left[ \mathcal{U}_t^{\otimes 2} \circ (\mathcal{N}_A \circ \mathcal{U}_{t-1}^{\otimes 2}) \circ \cdots \circ (\mathcal{N}_A \circ \mathcal{U}_1^{\otimes 2}) \left[ |\mathbf{0}\langle\mathbf{0}|_{AB}^{\otimes 2} \right] \mathcal{N}_A^\dagger \left( |x(t)\rangle\langle x(t)|_A^{\otimes 2} \right) \otimes_{j=1}^t \mathcal{N}_{B_j}^\dagger \left( |z_j\rangle\langle z_j|_{B_j}^{\otimes 2} \right) \right], \quad (\text{E7})$$

where the two-folded channel  $\mathcal{U} \otimes \tilde{\mathcal{U}}$  owns two copies of same unitary twirling but only one noisy channel on the second copy. As the local channels on bath systems  $\mathcal{N}_{B_1}, \dots, \mathcal{N}_{B_t}$  and last noisy channel on system  $\mathcal{N}_A$  are only followed by measurements without any further unitary operations, we adopt the adjoint channel map to isolate these channels from circuit dynamics, resulting in the last line. Here, we define  $\mathcal{N}_A \equiv \mathcal{I} \otimes \mathcal{N}_A$  for simplicity. As depolarizing channel is self-adjoint, we can immediately have

$$\mathcal{N}_B^\dagger \left( |z\rangle\langle z|_B^{\otimes 2} \right) = |z\rangle\langle z|_B \otimes \left( \gamma |z\rangle\langle z|_B + (1 - \gamma) \frac{\mathbf{I}}{d_B} \right) = \gamma |z\rangle\langle z|_B^{\otimes 2} + \frac{1 - \gamma}{d_B} |z\rangle\langle z|_B \otimes \mathbf{I}. \quad (\text{E8})$$

Furthermore, the inner product between  $|\hat{e}\rangle\langle\hat{e}|_B, |\hat{\tau}\rangle\langle\hat{\tau}|_B$  with this noisy projector is

$$\mathcal{N}_B^\dagger (|\hat{e}\rangle\langle\hat{e}|_B) = \left( \gamma |\hat{e}\rangle\langle\hat{e}|_B + \frac{1 - \gamma}{d_B} |\hat{e}\rangle\langle\hat{e}|_B \right) |\hat{e}\rangle\langle\hat{e}|_B = 1, \quad (\text{E9})$$

$$\mathcal{N}_B^\dagger (|\hat{\tau}\rangle\langle\hat{\tau}|_B) = \left( \gamma |\hat{\tau}\rangle\langle\hat{\tau}|_B + \frac{1 - \gamma}{d_B} |\hat{\tau}\rangle\langle\hat{\tau}|_B \right) |\hat{\tau}\rangle\langle\hat{\tau}|_B = \gamma + \frac{1 - \gamma}{d_B} \equiv g_B, \quad (\text{E10})$$

where we define  $g_B$  in the end for simplicity.

There are another two identities we need to introduce before the formal derivation, which is the noisy channel on identity and swap operators. For the identity operator, we simply have  $\mathcal{N}(|\hat{e}\rangle\langle\hat{e}|_A) = |\hat{e}\rangle\langle\hat{e}|_A$  since the depolarizing channel is unital. For the swap operator, we have

$$\mathcal{N}(|\hat{\tau}\rangle\langle\hat{\tau}|) = (\mathcal{I} \otimes \mathcal{N}) \left[ \sum_{i,j} |i, j\rangle\langle j, i| \right] = \sum_{i,j} |i\rangle\langle j| \otimes \mathcal{N}(|j\rangle\langle i|) \quad (\text{E11})$$

$$= \sum_{i,j} |i\rangle\langle j| \otimes \left( \gamma |j\rangle\langle i| + \frac{(1 - \gamma)\delta_{ij}}{d} \mathbf{I} \right) \quad (\text{E12})$$

$$= \gamma |\hat{\tau}\rangle\langle\hat{\tau}|_A + \frac{1 - \gamma}{d_A} |\hat{e}\rangle\langle\hat{e}|_A. \quad (\text{E13})$$

We now consider the Haar ensemble average of each circuit unitary to derive analytical results. Starting from  $t = 1$ , the unitary twirling of  $U_1$  on  $|\mathbf{0}\rangle\langle\mathbf{0}|_{AB_1}^{\otimes 2}$  followed by local noisy channels and bath measurements, we have

$$\begin{aligned} & \mathcal{N}_{B_1}^\dagger (\langle\langle z_1 |_{B_1}) \mathcal{N}_A [\mathbb{E}_{U_1 \in \text{Haar}} \mathcal{U}_1^{\otimes 2} (|\mathbf{0}\rangle\langle\mathbf{0}|_{AB_1})] \\ &= \frac{1}{d_A d_B (d_A d_B + 1)} \mathcal{N}_{B_1}^\dagger (\langle\langle \hat{e} |_{B_1}) [\mathcal{N}_A (|\hat{e}\rangle\langle\hat{e}|_A) |\hat{e}\rangle\langle\hat{e}|_{B_1} + \mathcal{N}_A (|\hat{\tau}\rangle\langle\hat{\tau}|_A) |\hat{\tau}\rangle\langle\hat{\tau}|_{B_1}] \end{aligned} \quad (\text{E14})$$

$$= \frac{1}{d_A d_B (d_A d_B + 1)} \mathcal{N}_{B_1}^\dagger (\langle\langle \hat{e} |_{B_1}) \left[ |\hat{e}\rangle\langle\hat{e}|_A |\hat{e}\rangle\langle\hat{e}|_{B_1} + \gamma |\hat{\tau}\rangle\langle\hat{\tau}|_A |\hat{\tau}\rangle\langle\hat{\tau}|_{B_1} + \frac{1-\gamma}{d_A} |\hat{e}\rangle\langle\hat{e}|_A |\hat{\tau}\rangle\langle\hat{\tau}|_{B_1} \right] \quad (\text{E15})$$

$$= \frac{1}{d_A d_B (d_A d_B + 1)} \left[ \left( 1 + \frac{1-\gamma}{d_A} g_B \right) |\hat{e}\rangle\langle\hat{e}|_A + \gamma g_B |\hat{\tau}\rangle\langle\hat{\tau}|_A \right]. \quad (\text{E16})$$

As both the identity and swap operators appear, we next turn to the transition matrix under local depolarizing noise. For twirling on identity, we have

$$\begin{aligned} & \mathcal{N}_{B_1}^\dagger (\langle\langle z_2 |_{B_2}) \mathcal{N}_A [\mathbb{E}_{U_2 \in \text{Haar}} \mathcal{U}_2^{\otimes 2} (|\hat{e}\rangle\langle\hat{e}|_A |\mathbf{0}\rangle\langle\mathbf{0}|_{B_2})] \\ &= \mathcal{N}_{B_1}^\dagger (\langle\langle z_2 |_{B_2}) \left[ \frac{d_A^2 d_B - 1}{d_B (d_A^2 d_B^2 - 1)} \mathcal{N}_A (|\hat{e}\rangle\langle\hat{e}|_A) |\hat{e}\rangle\langle\hat{e}|_{B_2} + \frac{d_A (d_B - 1)}{d_B (d_A^2 d_B^2 - 1)} \mathcal{N}_A (|\hat{\tau}\rangle\langle\hat{\tau}|_A) |\hat{\tau}\rangle\langle\hat{\tau}|_{B_2} \right] \end{aligned} \quad (\text{E17})$$

$$= \frac{d_A^2 d_B - 1}{d_B (d_A^2 d_B^2 - 1)} |\hat{e}\rangle\langle\hat{e}|_A + \frac{d_A (d_B - 1)}{d_B (d_A^2 d_B^2 - 1)} \left( \gamma |\hat{\tau}\rangle\langle\hat{\tau}|_A + \frac{1-\gamma}{d_A} |\hat{e}\rangle\langle\hat{e}|_A \right) g_B \quad (\text{E18})$$

$$= \left[ \frac{d_A^2 d_B - 1}{d_B (d_A^2 d_B^2 - 1)} + \frac{d_A (d_B - 1)}{d_B (d_A^2 d_B^2 - 1)} \frac{1-\gamma}{d_A} g_B \right] |\hat{e}\rangle\langle\hat{e}|_A + \frac{d_A (d_B - 1)}{d_B (d_A^2 d_B^2 - 1)} \gamma g_B |\hat{\tau}\rangle\langle\hat{\tau}|_A \quad (\text{E19})$$

$$\equiv m_{00} |\hat{e}\rangle\langle\hat{e}|_A + m_{10} |\hat{\tau}\rangle\langle\hat{\tau}|_A. \quad (\text{E20})$$

Similarly, we can derive the twirling on swap as

$$\begin{aligned} & \mathcal{N}_{B_1}^\dagger (\langle\langle z_2 |_{B_2}) \mathcal{N}_A [\mathbb{E}_{U_2 \in \text{Haar}} \mathcal{U}_2^{\otimes 2} (|\hat{\tau}\rangle\langle\hat{\tau}|_A |\mathbf{0}\rangle\langle\mathbf{0}|_{B_2})] \\ &= \mathcal{N}_{B_1}^\dagger (\langle\langle z_2 |_{B_2}) \left[ \frac{d_A (d_B - 1)}{d_B (d_A^2 d_B^2 - 1)} \mathcal{N}_A (|\hat{e}\rangle\langle\hat{e}|_A) |\hat{e}\rangle\langle\hat{e}|_{B_2} + \frac{d_A^2 d_B - 1}{d_B (d_A^2 d_B^2 - 1)} \mathcal{N}_A (|\hat{\tau}\rangle\langle\hat{\tau}|_A) |\hat{\tau}\rangle\langle\hat{\tau}|_{B_2} \right] \end{aligned} \quad (\text{E21})$$

$$= \frac{d_A (d_B - 1)}{d_B (d_A^2 d_B^2 - 1)} |\hat{e}\rangle\langle\hat{e}|_A + \frac{d_A^2 d_B - 1}{d_B (d_A^2 d_B^2 - 1)} \left( \gamma |\hat{\tau}\rangle\langle\hat{\tau}|_A + \frac{1-\gamma}{d_A} |\hat{e}\rangle\langle\hat{e}|_A \right) g_B \quad (\text{E22})$$

$$= \left[ \frac{d_A (d_B - 1)}{d_B (d_A^2 d_B^2 - 1)} + \frac{d_A^2 d_B - 1}{d_B (d_A^2 d_B^2 - 1)} \frac{1-\gamma}{d_A} g_B \right] |\hat{e}\rangle\langle\hat{e}|_A + \frac{d_A^2 d_B - 1}{d_B (d_A^2 d_B^2 - 1)} \gamma g_B |\hat{\tau}\rangle\langle\hat{\tau}|_A \quad (\text{E23})$$

$$\equiv m_{01} |\hat{e}\rangle\langle\hat{e}|_A + m_{11} |\hat{\tau}\rangle\langle\hat{\tau}|_A. \quad (\text{E24})$$

Combining Eqs. (E20) and (E24), we can summarize the noisy transition matrix as

$$\tilde{M} = \begin{pmatrix} m_{00} & m_{01} \\ m_{10} & m_{11} \end{pmatrix}, \quad (\text{E25})$$

and when  $\gamma = 1$  for noiseless circuit, the transition matrix  $\tilde{M}$  reduces to the transition matrix  $M$  in Eq. (C15) as expected.

The ensemble average of the sum in Eq. (E7) then becomes

$$\begin{aligned} & \mathbb{E}_{U \in \text{Haar}} P[\mathbf{z}(t), x(t)] \tilde{P}[\mathbf{z}(t), x(t)] \\ &= \frac{1}{d_A d_B (d_A d_B + 1)} \langle \underline{0} | \tilde{M}^{t-1} \left[ \left( 1 + \frac{1-\gamma}{d_A} g_B \right) |\underline{0}\rangle + \gamma g_B |\underline{1}\rangle \right] + \frac{1}{d_A d_B (d_A d_B + 1)} \langle \underline{1} | \tilde{M}^{t-1} \left[ \left( 1 + \frac{1-\gamma}{d_A} g_B \right) |\underline{0}\rangle + \gamma g_B |\underline{1}\rangle \right] g_A \end{aligned} \quad (\text{E26})$$

$$= \frac{1}{d_A d_B (d_A d_B + 1)} (\langle \underline{0} | + g_A \langle \underline{1} |) \tilde{M}^{t-1} \left[ \left( 1 + \frac{1-\gamma}{d_A} g_B \right) |\underline{0}\rangle + \gamma g_B |\underline{1}\rangle \right], \quad (\text{E27})$$

where we define  $g_A \equiv \gamma + (1-\gamma)/d_A$ . The overall expression is too complicated to present here, but in principle, one can evaluate Eq. (E27) as it is only a 2-dimensional linear system. Finally, we obtain at the noisy XEB fidelity as

$$\tilde{\mathcal{F}}_{\text{XEB}}(t) = 4^{N_A + t N_B} \mathbb{E}_{U \in \text{Haar}} P[\mathbf{z}(t), x(t)] \tilde{P}[\mathbf{z}(t), x(t)] - 1. \quad (\text{E28})$$

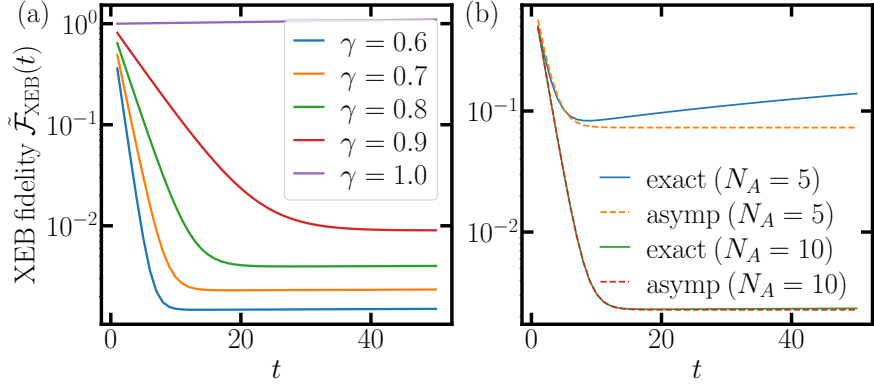


Figure 8. Noisy theory for XEB fidelity in HRCS. (a) We show the dynamics of noisy XEB theory of Eq. (E28) in a system of  $N_A = N_B = 10$  qubits with various depolarizing parameter  $\gamma$ . (b) We compare the exact noisy XEB theory of Eq. (E28) (solid) and asymptotic theory of Eq. (E29) (dashed) for  $N_A = 5$  and  $N_A = 10$ . Here we choose  $N_B = N_A$  and  $\gamma = 0.7$ .

In the large system and bath limit of  $d_A \gg 1, d_B \gg 1$ , we can simplify it to the form presented in the main text, and we also list it here for reference

$$\tilde{\mathcal{F}}_{\text{XEB}}(t) \simeq \gamma^{2t} \left( 1 + \frac{1 - \gamma}{\gamma d_B} t \right) + \frac{\gamma}{(1 - \gamma) d_A}. \quad (\text{E29})$$

In Fig. 8a, we plot the exact noisy XEB fidelity of Eq. (E28) in a system of  $N_A = 10$  and  $N_B = 10$  qubits. Via tuning the depolarizing channel parameter  $\gamma$ , we see different behaviors. For  $\gamma = 1$  (purple), we recover the dynamics of ideal XEB fidelity in HRCS, which can be simply derived from Eq. (C1). Meanwhile, once the noise exists with  $\gamma < 1$ , we first see an exponential decay in the XEB fidelity as expected due to the increase of circuit steps; With increasing time steps, the XEB fidelity approaches a plateau due to the repeated local measurements and statistical deviation of CP in HRCS. In Fig. 8b, we plot the exact theory in Eq. (E28) (solid lines) and asymptotic theory in Eq. (E29) (dashed lines) for comparison. Although the asymptotic theory of Eq. (E29) becomes singular at noiseless limit  $\gamma \rightarrow 1$ , here we mainly focus on the noisy region  $\gamma < 1$ . Indeed, with the increase of the system size  $N_A + N_B$ , we see a better agreement for the asymptotic approximation in finite temporal steps.

#### Appendix F: Additional details of experiments

In this section, we provide additional details of the experiments on IBM Quantum devices.

In the classical verifiable experiment of Fig. 2c in the main text, we implement a circuit of  $N_A = 5, N_B = 5$  qubits on the IBMQ Torino and in each step, we apply a  $L = 8$  layer parameterized circuit. Due to the automatic qubit allocation from Qiskit, for temporal steps  $t \leq 10$ , our circuit uses qubits shown in Fig. 9a (blue circuits) while for  $t = 13, 16$ , it uses qubits shown in Fig. 9b. In both cases, the circuit is applied on a line of 1D qubits and thus the two-qubit gates are only applied on nearest neighbors as we requested. In Fig. 10a, we show the number of native gates of IBMQ Torino used in our experiments for different  $t$  thus effective qubit number  $N_{\text{eff}}(t)$ , and the number of gates increases linearly with  $t$  as expected. For the largest temporal steps of  $t = 16$ , we use 5049 SX gates, 3684 RZ gates and 1152 CZ gates.

For the quantum supremacy experiment of Fig. 3 in the main text, as Qiskit allocates different qubits for each circuit instance, we do not show the qubits being used on IBMQ Torino here. Instead, we show the number of native gates in the circuits in Fig. 10b. Due to the fact of two patch circuit, the number of gates used in this experiment is roughly two times the one in Fig. 10a for the same  $t$ .

In Fig. 11, we present the typical circuit operation error rates and qubit lifetime in our experiment of Fig. 2c in the main text, provided by IBM Quantum. The top and bottom panels correspond to the experiments with  $t \leq 10$  and  $t = 13, 16$ . The detailed gate and readout error for each qubit can be found in the subplots, and we list the average error rate over used qubits, which are also presented in Methods. For  $t \leq 10$ , the average SX gate error is  $e_{\text{SX}} = (3.07 \pm 1.27) \times 10^{-4}$ , CZ gate error is  $e_{\text{CZ}} = (2.64 \pm 0.673) \times 10^{-3}$  and readout error  $e_{\text{read}} = (2.14 \pm 1.48) \times 10^{-2}$ . For  $t = 13, 16$ , the average SX gate error is  $e_{\text{SX}} = (3.38 \pm 1.86) \times 10^{-4}$ , CZ gate error is  $e_{\text{CZ}} = (2.39 \pm 0.382) \times 10^{-3}$  and readout error  $e_{\text{read}} = (2.36 \pm 1.55) \times 10^{-2}$ . The average qubit relaxation time for  $t \leq 10$  is  $T_1 = 146 \pm 51.2 \mu\text{s}$  and the average dephasing time is  $T_2 = 120 \pm 48.4 \mu\text{s}$ . For  $t = 13, 16$ , they are  $T_1 = 180 \pm 25.4 \mu\text{s}, T_2 = 131 \pm 49.9 \mu\text{s}$ .

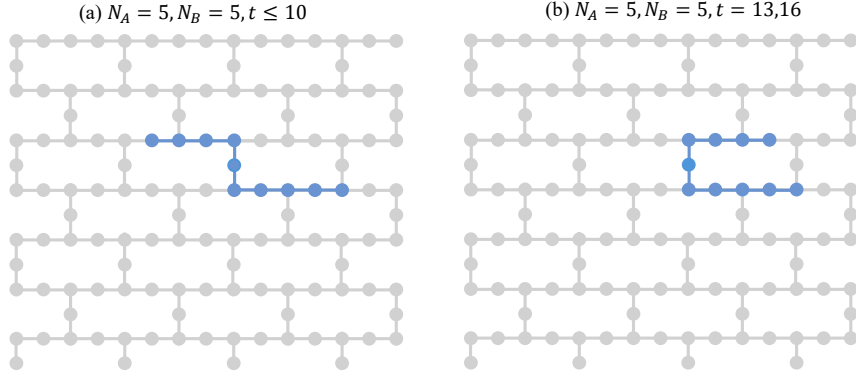


Figure 9. Circuit details in the experiment of Fig. 2c (main text). In (a) and (b), we plot the qubits that are used for the experiment with  $t \leq 10$  and  $t = 13, 16$  on IBMQ Torino.

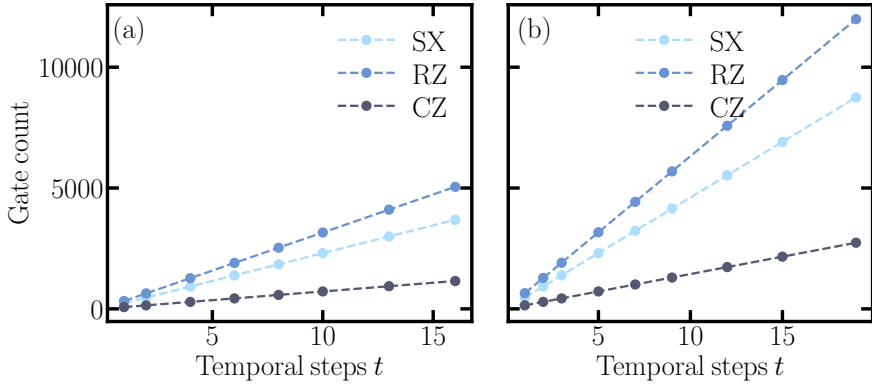


Figure 10. Number of SX, RZ and CZ gates used in experiments of Fig. 2c and Fig. 3 are shown in subplots a and b separately.

In the following, we detail the XEB fidelity in the patch circuit experiment. As the two patches are disjoint circuits, the joint sampling distribution can be factorized as  $P[\mathbf{z}_1(t), x_1(t), \mathbf{z}_2(t), x_2(t)] = P[\mathbf{z}_1(t), x_1(t)]P[\mathbf{z}_2(t), x_2(t)]$ . Therefore, when each patch has  $N'_A$  system and  $N'_B$  bath qubits, the ideal XEB fidelity of the two-patch circuit becomes

$$\mathcal{F}_{\text{XEB,patch}}(t) = (d_A d_B^t)^2 [Z_{\text{HRCS}}(t)^2] - 1 = \frac{4d_A^2 d_B^{2t} (d_A + 1)^{2(t-1)}}{(1 + d_A d_B)^{2t}} - 1, \quad (\text{F1})$$

where  $Z_{\text{HRCS}}(t)$  is the ensemble-averaged CP in HRCS with dimensions  $d_A = 2^{N'_A}$ ,  $d_B = 2^{N'_B}$  (see Eq. (C1)). In the large system limit of  $N'_A \gg 1$ , the ideal XEB fidelity scales as  $\sim 4 \exp \left[ \frac{2t(1-d_B^{-1})+d_B^{-1}-1}{d_A} \right] - 1$ , which still exponentially grows with temporal steps  $t$  but suppressed by the system dimension  $d_A$ . Similarly, the noisy theory for patch experiment becomes

$$\tilde{\mathcal{F}}_{\text{XEB,patch}}(t) = \left[ 1 + \tilde{\mathcal{F}}_{\text{XEB}}(t) \right]^2 - 1, \quad (\text{F2})$$

where  $\tilde{\mathcal{F}}_{\text{XEB}}(t)$  is the noisy theory of XEB fidelity for single HRCS in Eq. (E28) with dimensions  $d_A = 2^{N'_A}$ ,  $d_B = 2^{N'_B}$ .

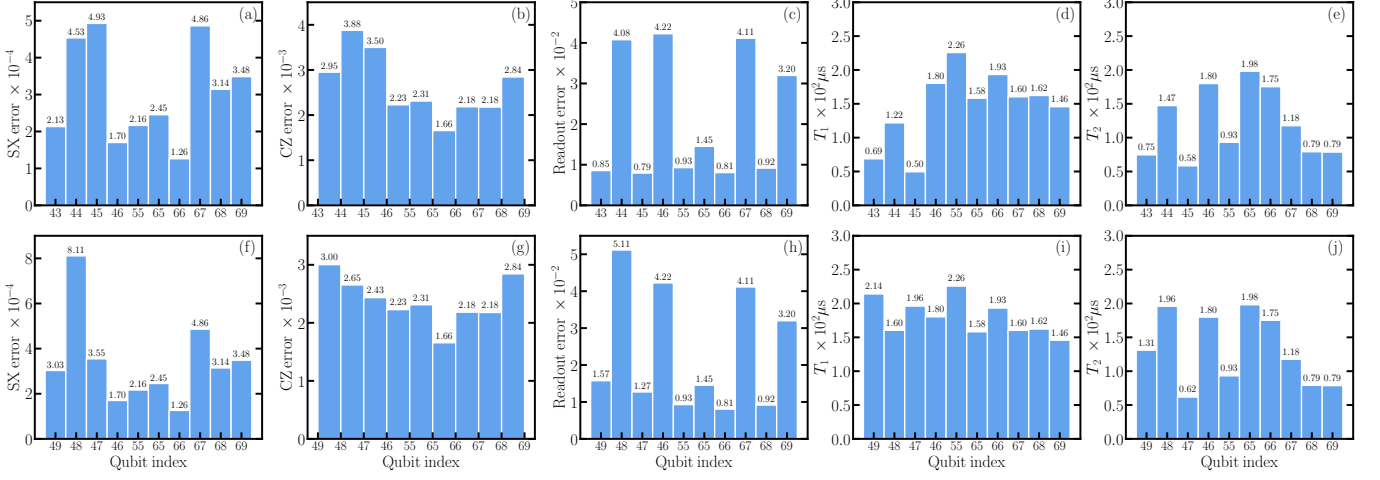


Figure 11. Circuit operation error rates and qubit lifetime in the experiment of Fig. 2c (main text). We list the SX error, CZ error, readout error, relaxation time  $T_1$  and dephasing time  $T_2$  of qubits. (a)-(e) correspond to experiments with  $t \leq 10$  and (f)-(j) correspond to experiments with  $t = 13, 16$ . In (a), (c), (f), (h), the bars show the error of the single qubit and in (b) and (g), each bar shows the error of the CZ gate connecting the qubit of left and right edges of the bar.